Manuscript File

https://doi.org/10.1016/j.margeo.2020.106216
© 2020. Licensed under the Creative Commons CC-BY-NC-ND 4.0 license
https://creativecommons.org/licenses/by-nc-nd/4.0/

Morphological controls and statistical modelling of boulder transport by extreme storms

Maria Alexandra Oliveira [a,b,c,*], Manuel G. Scotto [d], Susana Barbosa [e], César Freire de Andrade [b,f], Maria da Conceição Freitas [b,f]

[a] Centre for Ecology, Evolution and Environmental Changes, Faculdade de Ciências, Universidade de Lisboa, Lisbon, Portugal

[b] Instituto Dom Luiz, Faculdade de Ciências, Universidade de Lisboa, Lisbon, Portugal

[c] College on Polar and Extreme Environments (Polar2E), University of Lisbon, Portugal

[d] Departamento de Matemática and CEMAT, Instituto Superior Técnico, Universidade de Lisboa, Lisbon, Portugal

[e] INESC TEC - INESC Technology and Science, Porto, Portugal

[f] Departamento de Geologia, Faculdade de Ciências, Universidade de Lisboa, Lisbon, Portugal

[*] Corresponding author (Email address: maoliveira@fc.ul.pt)

Abstract

The study of coastal boulder accumulations generated by extreme marine events, and of the energy and frequency involved in boulder transport, is of paramount importance in understanding the risk associated with extreme marine inundations. One of the frequently asked questions is whether the deposits are storm or tsunami-related, both events being characterized by different return periods. Boulder transport by storms was monitored on the west coast of Portugal. Significant changes were detected in boulders' position as a result of extreme inundation by the 2013/2014 winter storms. Results presented in this work indicate that the wave power associated with the "Christina" and "Nadja" storms occur once every three years. However, this interval is not supported by field observations of boulder displacement, which suggests that wave power over-predicts boulder movement in the study area. Furthermore, wave parameters from the "Christina" and "Nadja" storms were very similar, but have generated different impacts in the boulder accumulation described herein. Differences include the magnitude and direction of boulder movement, and are most likely associated with distinct tidal levels during the events. Higher tide levels generated an increase in the sea surface level and thus in the reach of waves, which generated displacement of larger boulders and consequent cross-shore contribution in boulder transport. Regardless, the combination of monitoring campaigns, wave data, and statistical modelling of extreme values indicate that boulder transport by storms is more frequent than initially expected. Based on recorded boulder movements, we present a conceptual model for boulder ridge formation and development and identify significant

control of incoming flow by local geomorphological/topographical features. Storm events, not less frequent tsunamis, are identified as the events responsible for modulating this rocky coastline. These results question a direct attribution of coastal boulder deposits to tsunamis in coastal regions with a high risk of tsunami inundation.

Keywords: boulder ridges; geomorphological controls; wave power; peaks over threshold; rocky coastline; Portugal

1. Introduction

Coastal boulder deposits related to extreme marine events include rock particles with the intermediate axis ranging from 0.26m to 4.1m (Blair and McPherson, 1999), showing evidence of transport against gravity, directed upwards and inland. In rocky coastlines, they form conspicuous accumulations sitting on top of rock platforms (including shore platforms) and cliffs, forming various morphological features with different degrees of internal organization. Morphological features include boulder ridges (Williams and Hall, 2004; Cox et al., 2012), boulder clusters (Noormets et al., 2002; Switzer and Burston, 2010;

Paris et al., 2011; Biolchi et a., 2019a) and isolated boulders (Süssmilch, 1912; Oliveira et al., 2011; Paris et al., 2011). Boulder ridges comprise the most conspicuous morphology of boulder accumulations and are described as (Williams and Hall, 2004; Morton et al., 2008; Hall et al., 2008; Knight et al., 2009; Williams, 2010; Cox et al., 2012): (1) well organized clast-supported linear to arcuate structures developing along a shore-parallel to shore-normal direction; (2) forming asymmetrical cross-sections with steeper seaward faces; (3) showing a landward reduction in clast size, the largest clasts concentrating in the seaward slope, frequently imbricated. Organized boulder accumulations, in particular ridges, have been associated with inundation by both tsunami and storm waves (cf. Morton et al., 2008; Scheffers et al., 2009). In many cases, the nature (tsunami or storm) of the emplacement mechanisms and chronology of deposition is not obvious, especially in coastlines affected by both types of events. Storm and tsunami waves are intrinsically different, the most striking difference being the wave period: storm waves rarely exceed 15s. In comparison, tsunamis exceed 600s, which affects the duration of force acting on rock particles (Weiss and Diplas, 2015). The distinction between storm or tsunami origin is a highly debated issue in coastal geosciences (i.e., Switzer and Burston, 2010, Nandasena et al., 2011; Weiss, 2012; Marriner et al., 2017; Vött et al., 2019; Biolchi et al., 2019a). This differentiation has implications for coastal hazards and risk assessment, given that high magnitude storm and tsunami events are characterized by different return periods. For example, along the Western coast of Europe, including the Portuguese western coast, the recurrence intervals of extreme storms range from decades to centuries (e.g., Pires and Pessanha, 1986; Carvalho and Capitão, 1995), whereas high magnitude tsunamis occur separated by millennia (e.g., Cunha et al., 2012; Andrade et al., 2016). This distinction is especially relevant in areas with a high risk of tsunami inundation, such as the Portuguese coastline, which has been dramatically affected by the well-known transoceanic 1755 tsunami (Muir-Wood and Mignan, 2009), as well as subjected to high magnitude storms. (e.g., Daveau et al., 1978; Dominguez-Castro et al., 2013; Santos et al., 2014).

Cliff-top boulder accumulations with unknown origin have often been attributed to paleotsunamis due to their location above the reach of known storm waves, due to their large size and mass, and also based on the reconstruction of wave parameters from hydrodynamic equations (e.g., Young and Bryant, 1992; Young et al., 1996; Nott, 1997; Scheffers and Kelletat, 2005; Maouche et al., 2009). More recently, boulder movement in cliff-tops and shore platforms has been monitored during long-term surveys and unequivocally associated storm wave action (e.g., Williams and Hall, 2004; Hall et al., 2006; 2008; Hansom and Hall, 2009; Etienne and Paris, 2010; May et al., 2015; Kennedy et al., 2017; Cox et al., 2018; Biolchi et al., 2019b), thus challenging direct attribution of coastal boulder accumulations to tsunamis based solely on altimetry and boulder mass criteria. In line with these findings, inland and upward movement of large rock particles was detected in Portugal and elsewhere due to extreme inundation by waves from the extratropical storm in January 2014 (Santos et al., 2014; Autret et al., 2016; Oliveira, 2017, 2019; Cox et al., 2018).

Statistical modelling of extreme waves can be used as a tool to infer wave parameters with return intervals of 50 to 100-years, or higher, and these data contribute to the investigation of trends in storminess and extreme waves as well as on their impacts upon hard coastal engineering structures (Young et al., 2012). Statistical methods are usually focused on the most visible attribute of waves, their height (Ferreira and Soares, 1998; Soares and Scotto, 2001; Caires, 2016; Larsén et al., 2015), and, to a lesser extent, wave period, wind speed and water levels (Caires, 2016). However, statistical modelling can be further applied in the analysis of extremes by using other relevant sea-state parameters or variables representative of the wave regime at the site of interest (Ferreira and Soares, 1998). The capability of a wave-generated bore to reach further inland and produce boulder movement also depends on the wavelength (in turn related to the wave period) (see Lorang, 2002; Weiss, 2012). Furthermore, in low-lying cliffs of rocky coastlines with irregular profiles, wave run-up is strongly related to the offshore significant wave height and wavelength (Dodet et al., 2018). Therefore, we hypothesize that wave power, which incorporates both height and length, could be a possible proxy of the capability of a wave to generate boulder movement, both inland and upwards.

In agreement with the above, observations of boulder movement during present-day storms, and their wave power, can be further combined with statistical information derived from long-term time series of wave data to determine the return period of boulder displacement episodes. In this work, we investigate boulder transport by storm waves on a rocky coast on the west coast of Portugal, emphasizing the effects on an unusual storm cluster that impacted this coast in the winter 2013/2014. Based on field observations, we discuss the controls of storm-related boulder transport and how they modulate coastal boulder accumulations. Finally, we use observations, the computation of wave power during periods of boulder transport, and statistical modelling of wave power extremes to test wave power as a proxy for boulder movement.

2. Regional setting

The study area is located on the west coast of Portugal, approximately 40km northwest of Lisbon, in a coastline broadly trending North-South and fully exposed to the high-energy wave regime characterizing the North Atlantic Ocean (Fig. 1a-b).

2.1. Oceanographic forcing

Tides are semidiurnal, and, considering one Saros cycle, the highest astronomical spring tide reaches 1.8m amsl (above mean sea level); the mean spring tidal range is 2.8m (Instituto Hidrográfico, 1985-2003). According to data by Dodet et al. (2010a, b – see chapter 3. Data and Methods) deep water waves (herein described in terms of significant wave height, Hs, mean zero-crossing period, Tz, peak period, Tp, and peak wave direction, θp) essentially propagate from 260°-360° (Fig. 1c). The histogram of wave directions in Fig. 1c indicates that higher Hs and Tp associate, on average, with west-southwesterlies (directional interval 240°-260°) and west-northwesterlies (280°-300°), respectively. There is a 40° offset between directions corresponding to higher Hs and Tp (Fig. 1c). The plot of combined Hs and Tp shows a wide dispersion, suggesting that higher waves are not necessarily the longer, although they both preferably associate with the western octant (Fig. 1c and d). The directional distribution of wave power density, P (energy per second, and meter of wave crest), closely follows the Hs distribution (Fig. 1c).

Fig. 1 (a) Location of the study area on the SW European coastline; (b) location of the wave buoy, hindcast node and boulder deposit addressed in this study; background-image derived from the West-Iberian bathymetry model of Quaresma and Pichon (2013); (c) Wave direction histogram and average H_s, T_p and P for each direction class. (d) Plot of combined Hs and Tp. See Dodet et al. (2010a, b) for wave data at the hindcast node used in Fig. (c) and (d).

Deep-water wave data sets require further processing to account for wave transformation during propagation, including shoaling, refraction, diffraction, and coastal shelter effects (USACE, 2008). These transformations induce changes in wave height and direction, as well as convergence and divergence, and regulate the longshore distribution of wave power at the coast. Wave transformation matrices (WTM) are look-up tables containing graphical solutions of site-specific nearshore wave characteristics (cf. Deltares, 2016, Carapuço, 2016, and references therein). WTM are built considering all possible combinations of deep-water wave height and direction (2D matrices) relevant for the area under study and by running a numerical model of wave propagation over a suitable representation of the propagation domain. In this study, we used a WTM to address nearshore waves off the study area (Fig. 2). The matrix was prepared under a national monitoring project conducted by the Portuguese Ministry of Environment (Silveira et al., 2013). It contains information on changes in wave height (given by a multiplicative coefficient) and directional adjustments experienced by waves while traveling between deep-water and a target point in a water depth of 10m, at the latitude of the study area. The WTM was built using the deep-water wave series of Dodet et al. (2010a, b) and SWAN (Simulation WAves Nearshore) wave propagation model (Booji et al., 1999) developed by the Delft University of Technology (cf. Silveira et al., 2013).

Fig. 2: Wave transformation matrix for the nearshore of the study area, at a depth of 10m. Solid contour lines represent equal values of the height transformation coefficient; dashed lines represent the direction of propagation at the target point. Both input parameters, direction (Dir), and wave period (T) in axes refer to deep-water conditions. From Silveira et al. (2013)

The range in Hs of storm waves considered herein corresponds to breaking depths of 10-12 m. The location of the WTM target point is quite adequate to describe both scalar and directional parameters of incoming waves in near-breaking conditions. Examination of Fig. 2 clearly shows that shoaling effects dominate over refraction for a range of wave direction and peak period of storm waves addressed herein (260°-300° and >13s, respectively). The directional range at breaking is reduced (265°-280°), indicating that incoming wave bores will impact the study area at minimal angles. Moreover, at 10m depth, wave heights only slightly differ from deep water (transformation coefficient of 0.9 to 1.1). Altogether, this indicates that differences between deep-water and nearshore (local) wave characteristics are small and that deep-water data adequately describes local wave-induced hydrodynamic conditions.

The maximum increment in sea-level due to storm surge along the western Portuguese coast is typically less than 0.6m, and averages 0.4m (Taborda and Dias, 1992; Gama et al., 1997; Vieira et al., 2012). Storm climate is highly energetic, the number of storms per year, ranging from 9 to 12 (Ferreira et al., 2009). Storms last for 26 hours on average, reaching maximum Hs of about 14m and maximum peak period above 20s (Ferreira et al., 2009).

2.2 Coxos boulder deposit

A boulder deposit resulting from the deposition of large limestone clasts by extreme marine events (EME) has been identified north and south of Coxos beach (northern and southern sectors, respectively) (Oliveira, 2017) (Fig. 3a). In this region, the coastline broadly trends North-South, comprising small pocket sand beaches alternating with cliffs and stepped sub-horizontal structural platforms, cut in a marine to brackish carbonate sequence dated to the Lower Cretaceous (Rey, 2009) (Fig. 3b). The morphology of the rocky coast includes a crenulated plan-shape of the coastline, with pronounced indentations of the lower structural platforms and cliff face, and of cliff profiles, showing overhangs, benches, visors and pseudo-notches as well as stepped structurally-controlled surfaces. These irregularities result from differential erosion of alternating layers of limestone, claystone, sandstone and marl, gently dipping towards the southwest. Boulders are sourced in thick sedimentary sequences comprising sub-metric to metric limestone layers (0.5-1m thickness) interbedded with thin claystone layers (units C and D represented in Fig. 3a and b). The limestone layers (L17-L28) differ from each other in their composition (ranging from crystalline to sandy limestone), in fossil content, surface morphology, thickness, and joint frequency (Oliveira, 2017).

Fig. 3 (a) Geological units (A-E) outcropping in the study area, insets represented in Figure 4a; (b) Schematic log of the geological units (A-E)

The boulder accumulation addressed herein comprises over 1500 boulders showing evidence of transport against gravity, their source layers outcropping at lower altitudes, and seaward from their present-day location. Boulders are unevenly distributed in space, the southern sector comprising most particles. Therefore, this work will address the boulder accumulations found exclusively in the S sector. Boulders are parallelepiped in shape, they sit at 2-13m amsl, thus above tidal level, and their mass is under 30Mg. Boulders can be subdivided into three main populations based on their location, mass, source layer, distance from the bench edges, and morphology (Oliveira, 2017). Isolated boulders and imbricated boulder clusters, with a mass larger than 10Mg, are found at lower elevations (2-6m amsl), on top of unit C, and are mostly sourced in layer 19 (Fig. 3b and 4a and b). Further inland and upwards, on top of unit D, we frequently find isolated boulders and boulder clusters close to the bench edge, with mass ranging from 2.5 to 10Mg. A significant proportion of this population corresponds to fracture-bounded boulders detached from former overhangs formed by layer 28, as indicated by the unequivocal identification of the sockets with matching geometry (Fig. 5a).

Fig. 4: (a) Spatial distribution of boulder mass in the southern sector; insets represented in Figures 8a and b. (b) Cross-sections showing general outcropping lithology and position of the boulders over the low cliffs and

stepped sub-horizontal structural platforms; msl-mean sea level; mhwl-mean high-water level.

However, the most prominent features observed within this EME deposit correspond to ridges (Fig. 4a and Fig. 5b and c). They are elongated clast-supported accumulations, roughly aligned N-S to NE-SW, preferably developing inland of pronounced indentations affecting the structural platforms (Fig. 4a). They share some of the characteristics of the ridges found in the Aran Islands (Ireland) and described by Williams and Hall (2004) and Cox et al. (2012), such as asymmetric cross-sections, landward reduction in clast size and imbricated boulders in the seaward face (Fig. 5c). Boulders bordering the ridges range in mass from 1 to 2.5 Mg, while boulders on top of the ridges, and on the leeward side, rarely reach 1Mg (Fig. 4a). These structures are persistent in aerial imagery (available from the late 1940s onwards), although there is evidence of individual particles having been added to the ridges and others removed (Oliveira, 2017) (Fig. S1 and S2 in supporting information).

Weathering and washing out of soft marl and sandstone layers outcropping at higher altitudes originated colluvium deposits that partially bury some of the boulders (Fig. 5c).

Fig. 5: (a) Photograph facing South with isolated boulders, boulder sockets, and unit D topped by layer 28. (b) Photograph facing East of a boulder ridge. (c) Photograph facing Northeast of a boulder ridge with imbricated clasts in the seaward slope and colluvium deposit filling the voids between boulders. Vertical scale of 1m.

3. Data and Methods

In this work, we integrate observations of boulder movement (including transport distance and direction, as well as boulder mass) driven by present-day storm waves, tidal data synoptic of those storms, and statistical parameters of the wave regime computed from a long-term hindcast time series of wave data offshore Portugal. Present-day storm waves were characterized using data retrieved from the Leixões wave buoy (Fig. 1b).

3.1 Boulder movement

Boulders' initial position, before dislocation by storm waves, corresponds to the location measured during initial boulder mapping undertaken from 2009 to 2010. Boulder movement induced by present-day storms was acknowledged based on eyewitness accounts (one case) and by comparing boulders' initial and post-transport positions. The latter was recorded in field surveys in January and

February 2014, in the aftermath of “Christina” and “Nadja” storms. Surveys mainly focused on acquiring positions of particles displaced by storm waves during January and February 2014 and previously mapped in different locations. Besides, “new” particles were also mapped, i.e., boulders detached and emplaced by waves during this period and, whenever possible, the location from which they have been dislodged (sockets) (Fig. 6). The position of 280 boulders was monitored, corresponding to ~18% of the 1500 boulders initially mapped.

Fig. 6 (a) Photograph and (b) explanatory drawing of an 11Mg boulder that was dislodged, rotated, and pushed upwards by “Nadja” storm waves (February 2014). (c) Two boulders (outlined), with mass ranging from 0.5 to 0.9Mg, transported 20m towards SE over a structural platform, and placed on top of a boulder ridge by “Nadja” storm waves (February 2014).

Measurements taken during the monitoring surveys include the geographic location of the corners of each boulder’s largest surface and sockets of new boulders. This information was acquired using Real-Time Kinematic Global Positioning System equipment (mean accuracy better than 5cm). Boulder thickness was also measured using a measuring tape. Oven-dried rock samples were weighted to determine rock mass density by laboratory measurement of the volume of dislocated water. The corners of each boulder were transformed into a 3D surface, corresponding to the largest exposed boulder surface using geographical information system (GIS) software. Boulder mass was determined for each particle by combining the area of boulder surface (computed using GIS software) with boulder thickness and rock mass density. The information collected was assembled in a database containing data on mass, direction of movement, and travelled distance (taken as the shortest distance between socket and each displaced boulder).

3.2 Wave data

The long-term hindcast wave data used in this work corresponds to a 56-year (1953-2009) time series computed by Dodet et al. (2010a, b) using the third-generation spectral wave model WAVEWATCH III™. Hindcast results were validated using synoptic observations of 5 buoys located in deep water off the west and north coast of the Iberian Peninsula together with data from an Ocean Weather Station located off the coast of Ireland (Dodet et al., 2010b). Comparison of model results with observations revealed overall good agreement, with root mean square errors (RMS) of 0.50m for Hs, 20° for mean wave direction (Mwd), and 2s for Tp. These results were significantly improved by averaging the dataset over one month (RMS of 0.15m, 5°, and 1s, respectively). Model parameterization is further detailed in Dodet et al. (2010b). We used hindcast data extracted for a nodal point located off the central west coast of Portugal (see Fig. 1b for node location). The data comprises 6-h time series of Hs, Mwd, Tz and Tp over a box extending from 0° to 25°W and 30° to 60°N.

Parameters of storm waves responsible for boulder movement were extracted from both the hindcast time-series (Hs and Tp) and the 6-h time series of Hs, Mwd, and Tz record of the Leixões deep-water wave-buoy, maintained by the Portuguese Hydrographic Survey (Instituto Hidrográfico) (Fig. 1b). Following the storm threshold commonly used in Portugal, storm events were defined as periods during which Hs remained consistently higher than 5m and included intervals of lower Hs, but shorter than 12h (cf. Costa and Esteves, 2009; Ferreira et al., 2009). Peak period data in the wave-buoy series was extrapolated based on a linear correlation between Tp and zero-crossing period (Tz) yielded by the hindcast data (Fig. 7) to ensure consistency between observations retrieved from models and observations.

Fig. 7 Scatter plot of hindcast Tz against Tp and linear trendline and equation relating both variables.

Wave power (P) was computed using linear wave theory (Komar, 1976), based on wave parameters from both the hindcast time-series and the wave buoy, as described below:

$$P = ECn, \tag{1}$$

$$E = \frac{1}{8}\rho g {H_{rms}}^2, \tag{2}$$

$$C = \frac{g}{2\pi}T_p, \tag{3}$$

$$H_s = 1.416H_{rms} \tag{4}$$

Where E represents wave energy density (Jm^{-2}), C is wave celerity (ms^{-1}), n is the ratio between group velocity (C_g) and C (approximately 1/2 in deep-water conditions), ρ is water mass density (taken as $1025 kg \cdot m^{-3}$), g the acceleration of gravity ($9.81 m \cdot s^{-2}$). Hrms represents the square root of the average of the squares of all wave heights, which relates to Hs through equation (4) (USACE, 2008).

Tidal level, available at Instituto Hidrográfico (2010-2015), was also collected for days during which boulder movement was detected.

3.3 Statistical Modelling

Estimation of extreme values is commonly undertaken by one of two approaches (Caires, 2016): (i) fitting the generalized extreme value (GEV) distribution to annual maxima (AM), and (ii) fitting the generalized Pareto distribution (GPD) to peaks over a threshold (POT). Modelling using only block maxima is considered a wasteful approach when an entire data-series is available (Coles, 2001; Beirlant, 2004). The inclusion of more observations in the estimation of the GPD parameters using the POT method contributes to decreasing variance and more accurate estimates than the AM/GEV approach for data series with less than 100 years (Caires, 2016).

For a given sequence of independent and identically distributed (iid) random variables with unknown distribution function F, and considering as an extreme event all observations X_i's that exceed threshold u, the distribution of exceedance follows the GPD and is represented by the following expression (Coles, 2001; Beirlant et al., 2004):

$$H(x; u, \xi, \sigma) = P(X \leq x | X > u) = \begin{cases} 1 - \left(1 + \xi \dfrac{x-u}{\sigma}\right)^{-1/\xi}, & \xi \neq 0 \\ 1 - e^{-\frac{x-u}{\sigma}}, & \xi = 0 \end{cases} \quad (5)$$

Where $\xi \in \mathrm{R}$ and $\sigma > 0$ represent the shape and scale parameters, respectively. It is worth noting that in equation (5), σ is a function of u (Coles, 2001).

Although most of the statistical techniques provided by extreme value theory rely upon iid sequences, they can also be applied to dependent data as long as the inherent dependence is not strong enough to hinder the asymptotic normality of the test statistics and estimators adopted.

In practice, the choice of a suitable threshold value is frequently difficult. The use of the mean excess plot function (MEF) is useful for determining the threshold, say u_0, such that for $u > u_0$, $P(X > x + u|X > u) \approx (1+\xi x/\sigma)^{-1/\xi}$. The MEF is defined as being $E(X - u|X > u)$ and equals to $(\sigma + u\xi)/(1 - \xi)$ if $X \sim GPD(\xi,\sigma)$. In that case, for $u > u_0$, the plot of the sample MEF as a function of u should approximate a straight line above the u-level. After selecting the threshold, ξ and σ can be estimated resourcing to maximum likelihood methods.

The GPD was fitted to data on Hs, Tp and P extracted and computed from the hindcast series. Estimation of function parameters was undertaken resourcing to the “ismev” package from the R statistical software (R Core Team, 2017; Heffernan and Stephenson, 2018). Estimations of return values at 95% confidence interval, and of return periods (based on the cumulative probability approach) was achieved using the “lmomco” package (Asquith, 2018).

4 Results

4.1 Boulder movement during present-day storms

Storms responsible for boulder entrainment, transport, and placement are listed in Table 1. Detachment, transport, and emplacement of at least one 22Mg boulder close to the southernmost limit of the southern sector was eye-witnessed and reported to have occurred on March 10, 2003. The most probable socket area is located 2m amsl, at the edge of the bench formed by unit C. The boulder was transported towards SE, about 3.5m inland, and 2m upwards from the probable source. The 2003 storm waves were moderate in height (Hs of 5.6m), but peak periods were extremely high, up to 19.5s, maximum values of Tp coinciding with Hs maximum of 6 m. This information indicates that boulder movement in the study area can be triggered by deep water wave power magnitude ≥$2.97 \times 10^5 Wm^{-1}$.

Table 1: Offshore wave parameters, tidal level, and duration of storms associated with boulder movement in the study area.

Day (Storm name)	H_s (m)	T_m (s)	T_p (s)	P ($\times 10^5 Wm^{-1}$)	Storm duration (hours)	Tidal level (m amsl)
10-03-2003	5.6	16.9	19.5	2.97	18.7	0.64
03-01-2014 ("Christina")	9.0	14.6	16.7	6.62	90	0.00
27-01-2014	8.9	13.7	15.8	6.24	67	1.12
02-02-2014 ("Nadja")	9.0	14.0	16.1	6.36	36	1.90
05-02-2014	8.75	12.0	13.95	5.23	68	1.25
08-02-2014	8.5	13.0	15.0	5.31	65	0.00
15-02-2014	8.5	13.0	15.0	5.31	49	0.00

More recently, during January and February 2014, a cluster of storms caused significant boulder dislodgement along structural platform edges, as well as transport of boulders previously sitting on platforms, in both cross-shore and along-shore directions. The effects of wave impacts alternated between erosion and accumulation, abruptly changing within a few meters (Fig. 8).

Fig. 8 (a) (b) Boulder movement and erosion induced by the January and February storms. For location see Fig 4

These effects were mostly observed inland of structurally controlled indentations affecting the edge of the lower structural platform and toe of the cliff (Fig. 3b and Fig. 8). The amount of transport and removal of boulders previously resting over the rocky platform precluded the identification of boulder characteristics and direction of movement in some cases, particularly in the central segment of the southern sector. Here, structural platforms are narrower, the bench formed by unit D is practically absent, and the surface topping unit C reaches, in places, no more than 10m (CS1 in Fig. 4c). Similarly, the colluvium is also narrower, and boulder ridges, when existing, are poorly developed.

Further south, where the platform widens and the boulder ridges and colluvium deposit are developed, removal of a significant number of boulders bordering the boulder ridges over the highest structural platform was observed, generating a decrease of up to 5m in the localized width of those features (Fig. 8). Over the upper structural platform, boulders sitting at 8-13m amsl, with mass up to 6.5Mg, were moved both cross- and along-shore. Cross-shore transport was directed towards East (landward), produced maximum horizontal displacement of 20m, and maximum upward displacement of 3m. Alongshore transport was directed southwards, closely following the pending direction of the structural surface, reaching a maximum distance of 23m. Over the upper surface, the largest transported boulder (11Mg) was sourced in layer 28, detached from the platform edge, dislodged, rotated, and pushed upwards (Fig. 6a). Here, new boulders were mostly added to the ridges' slope facing the ocean, and also on top of ridges. That was the case for two boulders, represented in Fig. 6b, with mass ranging from 0.5 to 0.9Mg. These particles were detached from layer 26 and placed on top of a ridge, 1.5m higher, and 20m away from their source. These clasts showed no sign of impact or abrasion, nor did the structural surface from socket to ridge. This indicates that contact between the boulders and the bedrock was minimum, suggesting a mode of transport by saltation. Boulders bordering the ridges transported alongshore, were frequently found rolled over their long axis and showed, on occasion, signs of abrasion, suggesting transport by rolling. However, no clear markings were detected over the bedrock.

Over the lowest structural platform, topping unit C, boulder transport was detected in two situations. The largest boulder with a mass of 13Mg was detached from its socket, pushed upwards more than 3m, turned over and rotated 180°. The second movement was detected for a 10Mg boulder, previously part of an imbricated boulder cluster trapped in a joint-defined gully. This boulder was transported alongshore, reaching the maximum horizontal displacement of 110m. Transport occurred over the structural surface topping unit C, at ~3m amsl. Several linear scraping marks were found over the bedrock surface, following the boulder’s path, and suggesting that the principal mode of transport was sliding. Evidences of inundation throughout the platform were detected by the erosion of the colluvium. However, the boulders incorporating developed ridges, were left untouched.

Overall, 135 movements were detected by 98 boulders (some moved more than once), 67 of which have disappeared, most probably having been washed back to the sea. Also, 27 new boulders were found and measured, most having originated at the rock platform/cliff edges. Some were identified in previous surveys, has joint-bounded clasts, already unattached from the limestone layer but still in situ, having been removed by wave action during the 2014 storms (Fig. S3 in supporting information).

Between January and February of 2014, six storms occurred (Fig. 9). Significant wave height ranged from 8.5 to 9m, peak period from 14.0 to 16.7s, and wave power from 5.23×10^5 to $6.62\times10^5 Wm^{-1}$. Tidal level coinciding with storm peak ranged from 0 (mean sea level) to 1.9m amsl. Maximum values for Hs, Tp, and P were observed during storms “Christina” (3-7 January of 2014) and “Nadja” (1-2 February of 2014). Following the “Nadja” decline, boulder transport persisted in association with later storms (Table 1 and Fig. 9).

Fig. 9 Wave data from Leixões buoy and tidal level during January and February of 2014. Light-grey bands identify storm duration, and dark-grey lines overlap peaks in Hs and Tp.

The maximum tidal level occurred during the “Nadja” storm, on February 2, 2014. Peaks in Hs and Tp coincided with a high spring tide, which reached 1.9 m amsl. The movement of 42 boulders was attributed to either “Christina” or “Nadja” storm waves. Differences between patterns of mobilization during each of these storms comprised both magnitude and direction, and include (Fig. 10): (1) average mass of displaced boulders larger during “Nadja”; (2) higher vertical and horizontal transport distances associated with “Nadja”; (3) cross-shore transport was more frequent than alongshore transport (following the pending of the structural platform) during “Nadja”, the opposite occurring during “Christina”.

Fig. 10 (a) Scatter plot showing horizontal (Δx) versus vertical (Δz) boulder dislocation during January and February of 2014. Boulder mass is proportional to bubble size. (b) Wind-rose diagram showing direction of boulder movement during January and February 2014

4.2 Statistical modelling of extreme values

Parameters’ point estimates and return levels for Hs, Tp, and P are presented in Table 2. These results reveal that the value of the shape parameter is zero for all three variables, indicating that the underlying distribution function belongs to the Gumbel domain of attraction. The Gumbel domain contains a large variety of distributions ranging from moderately heavy (such as the log-normal distribution) to light (such as the normal distribution), regardless including or not a finite right endpoint. Hence, the next step was to assess whether the underlying distributions exhibited a finite right endpoint or not. To address this issue, we applied the two statistics introduced by (Neves and Pereira, 2010) that allow to distinguish distribution functions with finite right endpoint from those with infinite endpoint in the Gumbel domain of attraction. The results lead us to conclude that the assumption of finite right endpoint is tenable in all three cases.

Table 2: Parameters (scale and shape), point estimates, and standard errors (bracketed values) for Hs, Tp, and P. Return values and 95% confidence intervals for several time-periods. *values $\times 10^5$

		Hs	Tp	P
Threshold		7.4m	18s	5.1*
N		188	153	75
Parameters	Scale	0.789 (0.079)	0.714 (0.085)	1.108* (0.234*)
	Shape	0.049 (0.068)	0.011 (0.087)	0.1934 (0.101)
Return Values	2yr	7.95 (7.86, 8.05)	18.49 (18.40, 18.59)	6.08* (5.80, 6.36)
	5yr	8.72 (8.52, 8.92)	19.16 (18.97, 19.35)	7.49* (6.90, 8.08)
	10yr	9.31 (9.02, 9.61)	19.66 (19.39, 19.93)	8.64* (7.73, 9.55)
	20yr	9.94 (9.51, 10.37)	20.15 (19.77, 20.53)	9.87* (8.46, 11.28)
	50yr	10.79	20.85	11.63*

		(10.09, 11.50)	(20.19, 21.52)	(9.14, 14.11)
	100yr	11.47 (10.47, 12.47)	21.37 (20.43, 22.31)	13.06* (9.40, 16.72)

Swell waves with Hs of 5.6m (such as observed during March 2003) are extremely frequent, occurring on average 20 times per year. However, Tp of 20*s* (as recorded during the same storm) occurs on average only once every ten years. Wave power, corresponding to the combination of Hs and Tp observed in March 2003, was estimated to $2.97\times10^{5}Wm^{-1}$, and this condition occurs on average eight times per year.

“Christina” and “Nadja” were responsible for generating widespread changes in the Coxos deposit. Storm waves added some new boulders (including both small and large elements) to rock platforms, close to their seaward edge, and numerous boulders were added to pre-existent ridges. They also removed other particles, including isolated boulders and boulders bordering ridges. Smaller particles previously scattered over the platforms were washed out, except for a few clusters that resisted the impact and flow velocity of wave bores. Both “Christina” and “Nadja” raised very high and long waves, the Hs reaching 9m, which is a condition that occurs on average once every seven years. In turn, Tp exceeded 16s, a condition that occurs, on average, more than eight times a year.

Wave power resulting from the combination of Hs and Tp was estimated at over $6.3\times10^{5}Wm^{-1}$, which occurs once every ~3 years.

Figure 11 represents a wave matrix containing all combinations of Hs and Tp, and associated return periods obtained for the wave power (Fig. 11). The matrix may be divided into three regions, corresponding to contrasting magnitudes of wave power) and the size of return intervals. Sea state conditions correspondent to lower P values, below which no boulder movement was recorded, are represented in the upper left region of the matrix (region A in Fig. 11). This region describes joint occurrences of Hs and Tp during storms that are frequently observed in this coast, their return period being smaller than one year, and P magnitude under $3.2\times10^{5}Wm^{-1}$. In this region of the matrix, Hs is lower than 7m (for $Tp \leq 12s$), this value decreasing to 6m for larger Tp (up to 16s).

Fig. 11 Wave matrix showing return periods based on probability of occurrence for different values of Hs and Tp (axis) and related wave power. Region A identifies storms that are unable or are scarcely able to generate boulder transport in the study area; Region B corresponds to frequently observed storms generating occasional and restricted boulder transport; Region C corresponds to storms that match or exceed wave power of

“Christina” and “Nadja”, generating widespread and significant boulder detachment, movement, emplacement, and erosion in the study area

Occasional boulder movement (involving few particles, and particularly those with smaller mass) was observed during storms associated with Hs of 6 to 7m (a range of Hs still typical along this coast) but higher than average Tp, in the range of 13 to 17s. This condition is represented by region B in Fig. 11. Occasional and localized boulder transport is also possible during storms characterized by lower Tp, but higher Hs (8 to 11m) are required to reach wave-power ranging from $2.97-6.36\times10^5 Wm^{-1}$. The return period for these events was calculated in the range under one year up to ~ three years.

The right bottom region of the matrix (region C in Fig. 11) represents storms generating $P \geq 6.36\times10^5 \mathrm{Wm}^{-1}$. These events originated widespread displacement of boulders, significant changes in boulder positions (including washing out of numerous particles), detachment of rock particles from the cliff/bench edges leading to “new” particles. These effects have been observed in relation to “Nadja” and “Christina” storms and affected particles of variable mass located in the full range of elevation of the pre-existing boulder accumulation. However, boulder movement rarely occurred near the inner edge of the highest structural platform, except for the central segment, inland of a large indentation, where the platform is narrow. In addition, no boulder movement was detected in the leeward side of the ridges and was mostly detected in bordering particles. Storms matching “Nadja” and “Christina” in wave power occur on average once every ~3 years.

5 Discussion

5.1 Morphology and origin of the Coxos’ boulder accumulation

The Coxos boulder accumulation, due to its complexity and exposure to the high-energy wave regime characterizing the North Atlantic Ocean, offers a unique opportunity to understand how coarse clasts deposits develop in rocky coastline contexts. Foremost, the crenulated plan-shape of the coastline and cliff-face creates both macro and micromorphological features that influence energy dissipation from wave bores as they reach the coastline. In addition, a wide variety of boulder sizes are supplied by the varying layer thickness and joint frequency characterizing the outcropping sedimentary sequence, a conjugation amply described by Stephenson and Naylor (2011). This is further enriched by the structural geometry that provides several sub-horizontal surfaces at varying heights, ranging from 3m to 13m amsl. As a result of this complexity, there is a large variety in morphologies of coarse clast deposits, controlled in part by boulder size and by the distance from the coastline, ranging from isolated boulders to clusters and ridges.

Boulder movement detected during the 2013/2014 storms has revealed the dynamic character of the Coxos boulder accumulation. The development of different morphological features, particularly of boulder ridges, has shown to be the result of a continuous process, by the addition and removal of boulders over the study site. Large particles (>10Mg) were detached from bench edges and placed close to their socket by incoming wave bores. They suffered short vertical and horizontal transport distances (<2m) and came to rest as isolated boulders close to bench edges. Smaller particles, with mass ranging from 1 to 10Mg, were transported by rolling and sliding both cross-shore and alongshore, over surfaces of the structural platform until reaching an obstacle or being washed out. As boulders accumulated due to incoming bores, their largest surface faced the flow direction (stable hydraulic position), forming imbrication. Smaller boulders (<1Mg) were plucked from the bench edge and placed on top of boulder ridges, with minimum contact with the bedrock, suggesting a mode of transport of saltation. This continuous process allows boulder ridges to grow outwards and upwards until reaching a dynamic stability between erosion and accumulation, in response to the also dynamic character of the wave regime characterizing this region. As stated by Morton et al. (2008) and Weiss (2012), size trends, stratification, and organization of these morphological features are a result of short transport distances, of pre-existing obstacles (in this case boulder clusters or inner edge of the platform) and multiple high-frequency wave events, i.e., storms.

The description above is congruent with deposits formed by storm waves (rather than tsunamis) over a backstopped platform, the reasoning presented here is not only inferential but supported by field observations and wave tank experiments (cf. Cox et al., 2019). Features similar to Coxos' boulder ridges were observed by several authors in storm-related deposits elsewhere and described as accumulations of rock particles in contact with one another, several particles showing imbrications and exhibiting packed fabric, forming well-organized linear structures with asymmetrical cross-sections, consisting of a steep seaward face and a gentle down-flow slope (e.g., Williams and Hall, 2004; Morton et al., 2008, Hall et al., 2008; Cox et al., 2012, 2019). All these attributes are shared by Coxos' boulder ridges.

The orientation of the ridges, developing perpendicularly to indentations in the lower structural platform, are indicative of a strong geomorphological control of storm-related inundations over the structural surface. Although most ridges described in the literature preferably align parallel to the coast (e.g., Hall et al., 2006), shore-normal ridges have also been identified and associated with storm-related oblique wave attack (Knight et al., 2009). Geomorphological controls on inundations are challenging to model, regardless of the event responsible for deposition, and have been described elsewhere and reported by several authors. An example of geomorphological controls is the frequent location of boulder accumulations. These have been preferably found landward of vertical cliffs with narrow supratidal zones (Scheffers, 2004), inland of coastal indentations (Jones and Hunter, 1992; Suanez et al., 2009; Fichaut and Suanez, 2011), within joint-defined gullies (Knight et al., 2009; Knight and Burningham, 2011). Another example is clast imbrication closely related to joint-controlled channel orientation (Pérez-Alberti et al., 2012). Some features, such as indentations, generate local hotspots where the concentration of energy occurs, maximizing run-up and the chance of boulder dislodgement and transport (Jones and Hunter, 1992; Suanez et al., 2009; Canelas et al. 2014).

Despite the exceptional character of the 2013/2014 storms and the widespread boulder movement, boulders within well-developed ridges were left untouched, which indicates that the energy required to move those boulders must not have been reached during recent events. Given the high risk of tsunami inundation in the study area, one could invoke such an event to explain these features. In fact, several boulder accumulations found in the Portuguese rocky coastline have been attributed to the 1755 Lisbon tsunami inundation (e.g., Scheffers and Kelletat, 2005; Ramos-Pereira et al., 2009). Given the high energetic character and intensity of the 1755 tsunami (Muir-Wood and Mignan, 2009) and the size and height of the emplacement of the boulders, the consideration of a tsunami origin is not without reason. Furthermore, the boulder accumulation addressed herein, shares some of the characteristics described by Scheffers and Kelletat (2005) and Ramos-Pereira et al. (2009), such as boulder mass, elevation, and distance from the coastline.

Comparison of the Coxos' deposit with coarse-clast accumulations related to recent tsunami inundations is limited by the absence of observations in rocky coastlines. Paris et al. (2009) described imbricate boulder clusters and solitary clasts associated with the erosion of a rocky platform by the 2004 Indian Ocean Tsunami on the NW coast of Sumatra. However, Goto et al. (2007; 2010) did not find a size grading in space for tsunami deposits. However, the authors found exponential shoreward fining trends in storm-related deposits and attributed this behavior to the decrease in intensity of the forces associated with broken storm waves.

An alternative explanation for the untouched boulder ridges, is that storms more energetic than “Christina” and “Nadja”, with higher return periods, were responsible for the development of those features. Despite the exceptional character of the 2013/2014 winter storms (Masselink et al., 2016, and references therein), our knowledge of storm wave maxima is limited by the short instrumental records available (Cox et al., 2018). In fact, the geological record of western Europe has abundant evidences of considerable climatic variability on decadal to millennial timescales (Sorrel et al., 2012). So, it is reasonable to assume that extremer storms have occurred and that will occur again, albeit their lower frequency. In conclusion, it has become clear that, despite the devastation associated with recent tsunamis (Suppasri et al., 2012), storms may generate cumulative impacts that surpass those of tsunamis, due to their higher frequency (Marriner et al., 2017).

5.2 Statistical modelling of extreme storms

Different return periods obtained by considering only Hs or Tp illustrate the disparity of frequency estimations obtained by considering different parameters characterizing storm waves. Implications in computing return periods of storms exceeding some threshold of boulder movement are obvious.

Observation and measurement of boulder movement in the study area during present-day storms suggests that the magnitude of wave power associated with boulder transport during the 2003 swell, is 1.7 to 2.2 times lower than the values computed for all storm events identified during January and February 2014. The abnormal effects observed during the 2013/2014 storms are not unique to the Coxos beach boulder accumulation. They agree with observations of other boulder accumulations on the western coast of Europe (e.g., Autret et al., 2016; Cox et al., 2018). The 2013/2014 winter has been described as the most energetic period in the past 66 years, mostly due to a larger number of storms with close inter-event spacing, total storm duration, and extreme high water levels (Wadey et al., 2014; Masselink et al., 2016).

Even so, a low return period for boulder transport in the study area suggests that commonly observed storms are capable of generating boulder movement, and coarse clast transport in the study area is more frequent than initially anticipated.

However, “Nadja” storm has generated significant boulder transport and erosion of the deposit under analysis. These effects were neither observed during the four years preceding this storm, when initial field surveys were undertaken, nor have they been matched since then. The peculiar effects of this storm indicates that the amount of energy dissipated over the structural platform was atypical. Although statistical modelling indicated that storm wave heights, such as those observed during “Christina” and “Nadja”, occur once every seven years, the same does not happen for the peak period, with values occurring several times a year. More importantly, the return period obtained for wave power, which combines both wave height and period, suggests that these events occur on average once every three years. This recurrence interval is not supported by field observations of boulder displacement in the study area, and indicates that wave power over-predicts boulder movement in this region. These results are in line with the remarks of Weiss and Diplas (2015) and Erdmann et al. (2018)

regarding the risks of directly deriving hydrodynamic forces raised by wave impacts upon coastal boulders from deep-water wave parameters.

Considerable differences between the average mass and transport distance of displaced boulders were detected during “Christina” and “Nadja” storms, the latter reflecting a higher capability to detach and transport large particles. Given that wave parameters of both storms were identical, differences in transport magnitude must have been related with the coincidence of peak in storm intensity with peak tidal levels during “Nadja”. Higher tide levels increased sea surface height in 1.9m and, consequently, the reach of waves, thus increasing boulder transport capability of incoming bores. A comparison of the direction of boulder movement indicates a counter-clockwise rotation in the main transport direction during “Nadja”. Arguably, such a shift represents a relative increase in cross-shore transport over the structural platforms associated with wave swash due to a higher reach of waves. In turn, it resulted in a relative decrease in long-shore transport, mostly associated with backwash, following the natural pending of the structural platforms. Cross-shore boulder transport was responsible for adding boulders to the top of ridges, while longshore transport produced both erosion and outward growth of these structures. These interpretations are in line with other works that show the relevance of sea level in controlling the probability of overwash (Caires, 2016; Prime et al., 2016), this parameter in cases being more critical than wave height (Chini and Stansby, 2012).

Although boulder transport in the study area is quite frequent, the results above indicate that the effects induced by the February 2014 storms are not. Furthermore, this implies that the tidal level is an important variable to be considered when estimating return periods of the effects of extreme marine events. Ultimately, the return period of the effects observed during “Nadja” must be larger than those obtained solely based on wave power.

The incorporation of tidal level, wave parameters, and cross-shore profile is frequently modelled using wave run-up. Arguably, the determination of return periods for this parameter, instead of wave power, could render more realistic results. However, difficulties associated with the determination of run-up in complex rocky coastal contexts, associated with the influence of complex bathymetry and with the curvature and definition of the foreshore slope, are still unresolved (Dodet et al., 2018).

6 Conclusions

The Coxos boulder accumulation shares many characteristics with other deposits described in Northern Europe and associated with storms. The most conspicuous morphology are boulder ridges, which are dynamically stable features formed by successive adding/removal of boulders during both low and high magnitude events. Wave bores contribute to the outwards growth of ridges by adding boulders with mass <10Mg transported alongshore by rolling. The upward growth of these features is interpreted as a contribution from cross-shore transport of smaller boulders (mass <1Mg). These particles are detached from the bench edge, and directly placed on top of the ridge by saltation, facilitated by increased tidal levels.

Micro- and macro-morphological features, such as overhangs and indentations of the coastline, respectively, exert a strong influence in boulder detachment and transport over the structural platform.

Although wave power over-predicts boulder movement, restricted detachment and deposition of clasts during commonly observed storms suggest that this phenomenon is more frequent than initially anticipated and implies a dynamic character for coarse clast deposits in rocky coastline contexts.

Based on the results presented herein, there is no need to invoke a catastrophic event, such as a tsunami, to explain coastal boulder accumulations, in particular, boulder ridges. Higher and less frequent storms were probably responsible for the deposition of well-developed ridges that have been left untouched by the 2013/2014 storms.

7 Data Availability

Datasets related to this article can be found at: https://doi.pangaea.de/10.1594/PANGAEA.903857, an open-source online data Publisher for Earth & Environmental Science hosted at PANGAEA (Oliveira, 2019). Modelled wave data-series was downloaded from the MICORE project webpage (Dodet et al., 2010a), at http://disepla.fc.ul.pt/Micore/WaveDownload.html.

Acknowledgements

The authors would like to acknowledge Paula Marques Figueiredo for information regarding boulder transport in the study area and Alexandra Amorim, Anthony Kitchin, Catarina Lavinas, Diogo Carreira, João Nuno Silva, Mariana Ramos, Pedro Costa, Raquel Martins, Sandra Moreira, Tiago Silva and Vera Paio Lopes for field work assistance.

M. A. Oliveira was funded by FCT (Fundação para a Ciência e Tecnologia) through a PhD scholarship (SFRH/BD/66017/2009). This work was partially supported by; Instituto Dom Luiz through FCT financed program UID/GEO/50019/2013; and by the European NitroPortugal project: Strengthening Portuguese research and innovation capacities in the field of excess reactive nitrogen (EU H2020-TWINN-2015 692331).

This research is framed within the College on Polar and Extreme Environments (Polar2E) of the University of Lisbon.

References

Andrade, C. Freitas, M.C., Oliveira, M.A., Costa, P.J.M., 2016. On the sedimentological and historical evidences of seismic-triggered tsunamis in the Algarve coast of Portugal, in: Duarte, J., Schellart, W. (Eds)., Plate Boundaries and Natural Hazards - Geophysical Monograph 219, 1st edition, New Jersey, United States of America: American Geophysical Union and John Wiley and Sons, Inc, pp. 219-238. https://doi.org/10.1002/9781119054146.ch10

Asquith, W. (2018) lmomco-L-moments, censored L-moments, trimmed Lmoments, L-comoments, and many distributions. R package version 2.3.2.

Autret, R., Dodet, G., Fichaut, B., Suanez, S., David, L., Leckler, F., Ardhuin, F., Ammann, J., Grandjean, P., Allemand, P., Filipot, J.-F., 2016. A comprehensive hydro-geomorphic study of cliff-top storm deposits on Banneg Island during winter 2013–2014. Marine Geology 382, 37-55. https://doi.org/10.1016/j.margeo.2016.09.014

Beirlant, J., Goegebeur, Y., Segers, J., Teugels, J., 2004. Statistics of Extremes: Theory and Applications, John Wiley & Sons, Chichester.

Biolchi, S, Furlani, S., Devoto, S., Scicchitano, G., Korbar, T., Vilibic, I., Šepić, J., 2019a. The origin and dynamics of coastal boulders in a semi-enclosed shallow basin: A northern Adriatic case study. Marine Geology 411, 62-77. https://doi.org/10.1016/j.margeo.2019.01.008

Biolchi, S., Denamiel, C., Devoto, S., Korbar, T., Macovaz, V., Scicchitano, G., Vilibić, I., Furlani, S., 2019b. Impact of the October 2018 Storm Vaia on Coastal Boulders in the Northern Adriatic Sea. Water 11, https://doi.org/10.3390/w11112229

Blair, T.C., McPherson, J.G., 1999. Grain-size and textural classification of coarse sedimentary particles. Journal of Sedimentary Research 69, 6–19. https://doi.org/10.2110/jsr.69.6

Booij, N., Ris, R., Holthuijsen, L., 1999. A third-generation wave model for coastal regions. I Model description and validation. Journal of Geophysical Research 104, 7649–7666. https://doi.org/10.1029/98JC02622

Caires, S., 2016. A comparative simulation study of the annual maxima and the peaks-over-threshold methods. Journal of Offshore Mechanics and Arctic Engineering 138, 051601. https://doi.org/10.1115/1.4033563

Canelas, R., Oliveira, M., Crespo, A., Neves, R., Costa, P., Freitas, C., Andrade, C., Ferreira, R. 2014, Mathematical simulation of boulder dislodgement by high-energy marine flows in the western coast of Portugal. in: EGU General Assembly Conference Abstracts, volume 16, EGU2014-16081.

Carapuço, A.M.M, 2016. Improving the transfer of coastal scientific knowledge: from concept to implementation. PhD Dissertation, Universidade de Lisboa.

Carvalho, M.M., Capitão, R., 1995. Extreme wave heights off the western coast of Portugal. Proceedings of the 14th International Conference on Ocean, Offshore and Arctic Engineering, 9pp.

Chini, N., Stansby, P., 2012. Extreme values of coastal wave overtopping accounting for climate change and sea-level rise. Coastal Engineering 65, 27–37. https://doi.org/10.1016/j.coastaleng.2012.02.009

Coles, S., 2001. An Introduction to Statistical Modeling of Extreme Values, Springer-Verlag London.

Costa, M., Esteves, R., 2009. Clima de agitação marítima na costa Oeste de Portugal Continental. in: Comunicações das XI Jornadas Técnicas de Engenharia Naval. Lisboa, Portugal: Instituto Superior Técnico, p. 15.

Cox, R., Zentner, D.B., Kirchner, B.J., Cook, M.S., 2012. Boulder ridges on the Aran Islands (Ireland): recent movements caused by storm waves, not tsunamis. The Journal of Geology 120, 249–272. https://doi.org/10.1086/664787

Cox, R., Jahn, K.L., Watkins, O.G., Cox, P., 2018. Extraordinary boulder transport by storm waves (west of Ireland, winter 2013–2014), and criteria for analysing coastal boulder deposits. Earth-Science Reviews 177, 623-636. https://doi.org/10.1016/j.earscirev.2017.12.014

Cox, R., O'Boyle, L., Cytrynbaum, J., 2019. Imbricated coastal boulder deposits are formed by storm waves, and can preserve a long-term storminess record. Scientific Reports 9, 10784. https://doi.org/10.1038/s41598-019-47254-w

Cunha, T., Matias, L., Terrinha, P., Negredo, A., Rosas, F., Fernandes, R., Pinheiro, L., 2012. Neotectonics of the SW Iberia margin, Gulf of Cadiz and Alboran Sea: a reassessment including recent structural, seismic and geodetic data. Geophysical Journal International 188(3), 850-872. https://doi.org/10.1111/j.1365-246X.2011.05328.x

Daveau, S., Almeida, G., Feio, M., Rebelo, F., Silva, E., Sobrinho, A., 1978. Os temporais de Fevereiro / Março de 1978. Finisterra 13 (26), 236-260. (in portuguese)

Deltares, 2016. Tool - Wave Transformation Table (available at https://publicwiki.deltares.nl/display/BWN1/Tool%20-%20Wave%20Transformation%20Table) (accessed 13 Ago 2016).

[dataset] Dodet, G., Bertin, X., Taborda, R. 2010a. Download wave data, Micore project webpage, http://disepla.fc.ul.pt/Micore/WaveDownload.html, Accessed: 2019-06-20.

Dodet, G., Bertin, X., Taborda, R., 2010b. Wave climate variability in the North East Atlantic Ocean over the last six decades. Ocean modelling 31, 120–131. https://doi.org/10.1016/j.ocemod.2009.10.010

Dodet, G., Leckler, F., Sous, D., Ardhuin, F., Filipot, J.-F., Suanez, S., 2018. Wave runup over steep rocky cliffs. Journal of Geophysical Research: Oceans 123, 7185–7205. https://doi.org/10.1029/2018JC013967

Dominguez-Castro, F., Trigo, R.M., Vaquero, J.M., 2013. The first meteorological measurements in the Iberian Peninsula: evaluating the storm of November 1724. Climate Change 118, 443-445. https://doi.org/10.1007/s10584-012-0628-9

Erdmann, W., Kelletat, D., Scheffers, A., 2018. Boulder transport by storms – Extreme-waves in the coastal zone of the Irish west coast. Marine Geology 399, 1–13. https://doi.org/10.1016/j.margeo.2018.02.003

Etienne, S., Buckley, M., Paris, R., Nandasena, A.K., Clark, K., Strotz, L., Chagué-Gofff, C., Goff, J., Richmond, B., 2011. The use of boulders for characterising past tsunamis: lessons from the 2004 Indian Ocean and 2009

South Pacific tsunamis. Earth-Science Reviews 107 (1,2), 76-90. https://doi.org/10.1016/j.earscirev.2010.12.006

Etienne, S., Paris, R., 2010. Boulder accumulations related to storms on the south coast of the Reykjanes Peninsula (Iceland). Geomorphology 114, 55–70. https://doi.org/10.1016/j.geomorph.2009.02.008

Ferreira, J.A., Soares, C.G., 1998. An application of the peaks over threshold method to predict extremes of significant wave height. Journal of Offshore Mechanics and Arctic Engineering 120, 165–176. https://doi.org/10.1115/1.2829537

Ferreira, O., Vousdoukas, M., Ciavola, P., 2009. Micore review of climate change impacts on storm occurrence (open access, deliverable wp1. 4). http://www.micore.eu/file.php?id=4

Fichaut, B. Suanez, S., 2011. Quarrying, transport and deposition of cliff-top storm deposits during extreme events: Banneg Island, Brittany. Marine Geology 283, 36–55. https://doi.org/10.1016/j.margeo.2010.11.003

Gama, C., Taborda, R., Dias, J., 1997. Sobrelevação do nível do mar de origem meteorológica “storm surge”, em Portugal Continental, Colectânea de ideias sobre a zona costeira de Portugal, 131–149.

Goto, K., Chavanich, S.A., Imamura, F., Kunthasap, P., Matsui, T., Minoura, K., Sugawara, D., Yanagisawa, H., 2007. Distribution, origin and transport process of boulders deposited by the 2004 Indian Ocean tsunami at Pakarang Cape, Thailand. Sedimentary Geology 202, 821-837. https://doi.org/10.1016/j.sedgeo.2007.09.004

Goto, K., Kawan, T., Imamura, F., 2010. Historical and geological evidence of boulders deposited by tsunamis, southern Ryukyu Islands, Japan. Earth-Science Reviews 102, pp. 77-99. https://doi.org/10.1016/j.earscirev.2010.06.005

Hall, A., Hansom, J., Williams, D., Jarvis, J., 2006. Distribution, geomorphology and lithofacies of cliff-top storm deposits: examples from the high-energy coasts of Scotland and Ireland. Marine Geology 232, 131–155. https://doi.org/10.1016/j.margeo.2006.06.008

Hall, A.M., Hansom, J.D., Jarvis, J., 2008. Patterns and rates of erosion produced by high energy wave processes on hard rock headlands: The Grind of the Navir, Shetland, Scotland. Marine Geology 248, 28–46. https://doi.org/10.1016/j.margeo.2007.10.007

Hansom, J., Hall, A., 2009. Magnitude and frequency of extra-tropical North Atlantic cyclones: a chronology from cliff-top storm deposits. Quaternary International 195, 42–52. https://doi.org/10.1016/j.quaint.2007.11.010

Heffernan, J.E., Stephenson, A.G., 2018. ismev: An Introduction to Statistical Modeling of Extreme Values. R package version 1.42.

Instituto Hidrográfico (1985-2003) and (2010-2015) Tabelas de marés capítulo III Informação suplementar sobre marés (in portuguese) available at, http://www.hidrografico.pt/download-tabelas-mare.php. (Accessed 6 November 2015).

Jones, B. Hunter, I.G., 1992. Very large boulders on the coast of Grand Cayman: the effects of giant waves on rocky coasts. Journal of Coastal Research 8 (4), pp. 763-774.

Kennedy, A., Mori, N., Yasuda, T., Shimozono, T., Tomiczek, T., Donahue, A., Shimura, T., Imai, Y., 2017. Extreme block and boulder transport along a cliffed coastline (Calicoan Island, Philippines) during Super Typhoon Haiyan. Marine Geology 383, 65-77. https://doi.org/10.1016/j.margeo.2016.11.004

Knight, J., Burningham, H., Barret-Mold, C., 2009. The geomorphology and controls on development of a boulder-strewn rock platform, NW Ireland. Journal of Coastal Research SI56, 1646-1650.

Knight, J., Burmingham, H., 2011. Boulder dynamics on an Atlantic-facing rock coastline, northwest Ireland. Marine Geology 283 (1–4), 56–65. https://doi.org/10.1016/j.margeo.2010.07.008

Komar, P.D., 1976. Beach Processes and Sedimentation. Prentice-Hall, Inc.

Larsén, X.G., Kalogeri, C., Galanis, G., Kallos, G., 2015. A statistical methodology for the estimation of extreme wave conditions for offshore renewable applications. Renewable Energy 80, 205–218. https://doi.org/10.1016/j.renene.2015.01.069

Lorang, M.S., 2002. Predicting the crest heights of a gravel beach. Geomorphology 48, 87-101. https://doi.org/10.1016/S0169-555X(02)00176-9

Maouche, S., Morhange, C., Meghraoui, M., 2009. Large boulder accumulation on the Algerian coast evidence tsunami events in the western Mediterranean. Marine Geology 262, 96–104. https://doi.org/10.1016/j.margeo.2009.03.013

Marriner, N., Kaniewski, D., Morhange, C., Flaux, C., Giaime, M., Vacchi, M., Goff, J., 2017. Tsunamis in the geological record: Making waves with a cautionary tale from the Mediterranean, Science Advances 3, e1700485. https://doi.org/10.1126/sciadv.1700485

Masselink, G., Castelle, B., Scott, T., Dodet, G., Suanez, S., Jackson, D., Floc'h, F., 2016. Extreme wave activity during 2013/2014 winter and morphological impacts along the Atlantic coast of Europe. Geophysical Research Letters 43, 2135–2143. https://doi.org/10.1002/2015GL067492

May, S.M., Engel, M., Brill, D., Cuadra, C., Lagmay, A.M.F., Santiago, J., Suarez, J.K., Reyes, M., Brückner, H., 2015. Block and boulder transport in Eastern Samar (Philippines) during Supertyphoon Haiyan. Earth Surface Dynamics 3(3), 543-558.

Morton, R.A., Richmond, B.M., Jaffe, B.E., Gelfenbaum, G., 2008, Coarse clast ridge complexes of the Caribbean: a preliminary basis for distinguishing tsunami and storm-wave origins. Journal of Sedimentary Research 78 (9), 624-637. https://doi.org/10.2110/jsr.2008.068

Muir-Wood, R., Mignan, A., 2009. A phenomenological reconstruction of the Mw9 November 1st 1755 earthquake source, in: Mendes-Victor, L.A., Oliveira, C.S., Azevedo, J., Ribeiro, A. (Eds) The 1755 Lisbon Earthquake: Revisited, Springer, pp. 121–146. https://doi.org/10.1007/978-1-4020-8609-0_8

Nandasena, N.A.K., Paris, R., Tanaka, N., 2011. Reassessment of hydrodynamic equations: Minimum flow velocity to initiate boulder transport by high energy events (storms, tsunamis). Marine Geology 281, 70–84. https://doi.org/10.1016/j.margeo.2011.02.005

Neves, C., Pereira, A., 2010. Detecting finiteness in the right endpoint of light-tailed distributions. Statistics & Probability Letters 80, 437–444. https://doi.org/10.1016/j.spl.2009.11.021

Noormets, R., Felton, E.A., Crook, K.A.W., 2002. Sedimentology of rocky shorelines: 2 Shoreline megaclasts on the north shore of Oahu, Hawaii-origins and history. Sedimentary Geology 150, 31-45. https://doi.org/10.1016/S0037-0738(01)00266-4

Nott, J., 1997. Extremely high-energy wave deposits inside the Great Barrier Reef, Australia: determining the cause—tsunami or tropical cyclone. Marine Geology 141, 193–207. https://doi.org/10.1016/S0025-3227(97)00063-7

Oliveira, M.A., 2017. Boulder deposits related to extreme marine events in the western coast of Portugal. PhD Dissertation, Universidade de Lisboa.

[dataset] Oliveira, M.A., 2019. Boulder movement monitored during "Christina" and "Nadja" 2014 storms in the Coxos boulder deposit, West coast of Portugal. PANGAEA, https://doi.pangaea.de/10.1594/PANGAEA.903857

Oliveira, M.A., Andrade, C., Freitas, M.C., Costa, P., Taborda, R., Janardo, C., Neves, R., 2011. Transport of large boulders quarried from shore platforms of the Portuguese west coast. Journal of Coastal Research SI64, 1871-1875.

Paris, R., Wassmer, P., Sartohadi, J., Lavigne, F., Barthomeuf, B., Desgages, E., Grancher, D., Baumert, P., Vautier, F., Brunstein, D., Gomez, C., 2009. Tsunamis as geomorphic crises: Lessons from the December 26, 2004 tsunami in Lhok Nga, West Banda Aceh (Sumatra, Indonesia). Geomorphology 104, 59-72. https://doi.org/10.1016/j.geomorph.2008.05.040

Paris, R., Naylor, L.A., Stephenson, W.J., 2011. Boulders as a signature of storms on rock coasts. Marine Geology 283, 1-11. https://doi.org/10.1016/j.margeo.2011.03.016

Pérez-Alberti, A., Trenhaile, A.S., Pires, A., López-Bedoya, J., Chaminé, H.I., Gomes, A., 2012. The effect of boulders on shore platform development and morphology in Galicia, north west Spain. Continental Shelf Research 48, 122–137. https://doi.org/10.1016/j.csr.2012.07.014

Pires, H., Pessanha. L., 1986. Estima da distribuição de probabilidade dos valores extremos, utilizando séries climatológicas curtas. Separata da Revista do Instituto Nacional de Meteorologia e Geofísica 4 (3-4), 3-25 (in Portuguese).

Prime, T., Brown, J.M., Plater, A.J., 2016. Flood inundation uncertainty: the case of a 0.5% annual probability flood event. Environmental Science & Policy 59, 1-9. https://doi.org/10.1016/j.envsci.2016.01.018

Quaresma, L.S., Pichon, A., 2013. Modelling the barotropic tide along the west Iberian margin. Journal of Marine Systems 109-110, S3 – S25. https://doi.org/10.1016/j.jmarsys.2011.09.016

R Core Team, 2017. R: A Language and Environment for Statistical Computing, R Foundation for Statistical Computing, Vienna, Austria.

Ramos-Pereira, A., Trindade, J., Neves. M., Borges, B., 2009. Indicadores geomorfológicos de tsunamino Parque Natural do SW Alentejano e Costa Vicentina (Malhão). Publicações da Associação Portuguesa de Geomorfólogos VI, 51-56. (in Portuguese)

Rey, J. 2009. Stratigraphie séquentielle et séquences de dépôt dans le Crétacé inférieur du bassin Lusitanien, Ciências da Terra Procedia Special Issue VI. http://cienciasdaterra.novaidfct.pt/index.php/ctproc/article/view/257. (Accessed: 2019-07-09)

Santos, A., Mendes, A., Corte-Real, J., 2014. Impacto da tempestade Hércules, em Portugal. Finisterra-Revista Portuguesa de Geografia XLIX 98, 197– 220.

Scheffers, A., 2004. Tsunami imprints on the Leeward Netherlands Antilles (Aruba, Curaçao, Bonaire) and their relation to other coastal problems. Quaternary International 120, pp. 163-172. https://doi.org/10.1016/j.quaint.2004.01.015

Scheffers, A., Kelletat, D., 2005. Tsunami relics on the coastal landscape west of Lisbon, Portugal. Science of Tsunami Hazards 23, 3–16.

Scheffers, A., Scheffers, S., Kelletat, D., Browne, T., 2009. Wave-emplaced coarse debris and megaclasts in Ireland and Scotland: Boulder transport in a high-energy littoral environment. The Journal of Geology 117, 553-573. https://doi.org/10.1086/600865

Silveira, T., Taborda, R., Andrade, C., Silva, A.N., Carapuço, A.M., 2013. Caracterização do clima de agitação junto à costa. Relatório Técnico, Projeto Criação e implementação de um sistema de monitorização no litoral abrangido pela área de jurisdição da Administração da Região Hidrográfica do Tejo.

FFCUL/APA, I.P., p. 53. http://sniamb.apambiente.pt/infos/geoportaldocs/Politicas/Agua/Ordenamento/SistemasMonitorizacaoLitoral/E_1.1.7.b_Clima_agitao_costa.pdf (Accessed 25-04-2017). (in Portuguese)

Soares, C.G., Scotto, M., 2001. Modelling uncertainty in long-term predictions of significant wave height. Ocean Engineering 28, 329–342. https://doi.org/10.1016/S0029-8018(00)00011-1

Sorrel, P., Debret, M., Billeaud, I., Jaccard, S.L., McManus, J.F., Tessier, B., 2012. Persistent non-solar forcing of Holocene storm dynamics in coastal sedimentary archives. Nature Geoscience 5 (12), 892-896. https://doi.org/10.1038/ngeo1619

Stephenson, W.J., Naylor, L.A., 2011. Geological controls on boulder production in a rock coast setting: insights from South Wales, UK. Marine Geology 283(1-4), 12-24. https://doi.org/10.1016/j.margeo.2010.07.001

Suanez, S., Fichaut, B., Magne, R., 2009. Cliff-top storm deposits on Banneg Island, Brittany, France: effects of giant waves in the eastern Atlantic Ocean. Sedimentary Geology 220, 12–28. https://doi.org/10.1016/j.sedgeo.2009.06.004

Suppasri, A., Muhari. A., Ranasinghe, P., Mas, E., Shuto, N., Imamura, F., Koshimura, S., 2012. Damage and reconstruction after the 2004 Indian ocean tsunami and the 2011 great east japan tsunami Journal of Natural Disaster Science 34, 19–39. https://doi.org/10.2328/jnds.34.19

Süssmilch, C.A., 1912, Notes on some recent marine erosion at Bondi. Royal Society of New South Wales Journal and Proceedings 46, 155-158.

Switzer, A.D., Burston, J.M., 2010. Competing mechanisms for boulder deposition on the southeast Australian coast. Geomorphology 114, 42–54. https://doi.org/10.1016/j.geomorph.2009.02.009

Taborda, R., Dias, J.A., 1992. Análise da sobreelevação do nível do mar de origem meteorológica durante os temporais de fevereiro/março de 1978 e dezembro de 1981. Geonovas 1, 89–97. https://issuu.com/associacaoportuguesageologos/docs/apg_geonovas_especial1

USACE, 2008. Coastal engineering manual (CEM), engineer manual 1110-2-1100. https://www.publications.usace.army.mil/USACE-Publications/Engineer-Manuals/

Vieira, R., Antunes, C., Taborda, R., 2012. Caracterização da sobreelevação meteorológica em Cascais nos últimos 50 anos. Proceedings of the 2as Jornadas de Engenharia Hidrográfica, Lisbon, Portugal, 21-22. (in Portuguese)

Vött, A., Bruins, H.J., Gawehn, M., Goodman-Tchernov, B.N., De Martini, P.M., Kelletat, D., Mastronuzzi, G., Reicherter, K., Röbke, B.R., Scheffers, A., Willershäuser, T., Avramidis, P., Bellanova, P., Costa, P.J.M., Finkler, C., Hadler, H., Koster, B., Lario, J., Reinhardt, E., Mathes-Schmidt, M., Ntageretzis, K., Pantosti, D., Papanikolaou, I., Sansò, P., Scicchitano, G., Smedile, A. and Szczuciski, W. 2019. Publicity waves based on manipulated geoscientific data suggesting climatic trigger for majority of tsunami findings in the Mediterranean – Response to 'Tsunamis in the geological record: Making waves with a cautionary tale from the Mediterranean' by Marriner et al. (2017). Zeitschrift für Geomorphologie SI 62(2), 7-45. https://doi.org/10.1127/zfg_suppl/2018/0547

Wadey, M.P., Haigh, I.D., Brown, J.M., 2014. A century of sea level data and the UK's 2013/14 storm surges: an assessment of extremes and clustering using the Newlyn tide gauge record, Ocean Science 10, 1031–1045. https://doi.org/10.5194/os-10-1031-2014.

Weiss, R., 2012. The mystery of boulders moved by tsunamis and storms. Marine Geology 295-298, 28–33. https://doi.org/10.1016/j.margeo.2011.12.001

Weiss, R., Diplas, P., 2015. Untangling boulder dislodgement in storms and tsunamis: Is it possible with simple theories? Geochemistry, Geophysics, Geosystems 16, 890–898, https://doi.org/10.1002/2014GC005682

Williams, D.M., 2010. Mechanisms of wave transport of megaclasts on elevated cliff-top platforms: Examples from western Ireland relevant to the storm-wave versus tsunami controversy. Irish Journal of Earth Sciences 28, 13-23, Williams, D.M., Hall, A.M. 2004. Cliff-top megaclast deposits of Ireland, a record of extreme waves in the North Atlantic-storms or tsunamis? Marine Geology 206, 101–117. https://doi.org/10.1016/j.margeo.2004.02.002

Young, R.W., Bryant, E.A., 1992. Catastrophic wave erosion on the southeastern coast of Australia: Impact of the Lanai tsunamis ca. 105 ka? Geology 20 (3): 199-202. https://doi.org/10.1130/0091-7613(1992)020<0199:CWEOTS>2.3.CO;2

Young, R., Bryant, E.A., Price, D., 1996. Catastrophic wave (tsunami?) transport of boulders in Southern New South Wales, Australia. Zeitschrift für Geomorphologie NF 40, 191-207.

Young, I., Vinoth, J., Zieger, S., Babanin, A.V., 2012. Investigation of trends in extreme value wave height and wind speed. Journal of Geophysical Research: Oceans 117, C00J06. https://doi.org/10.1029/2011JC007753

Fig1

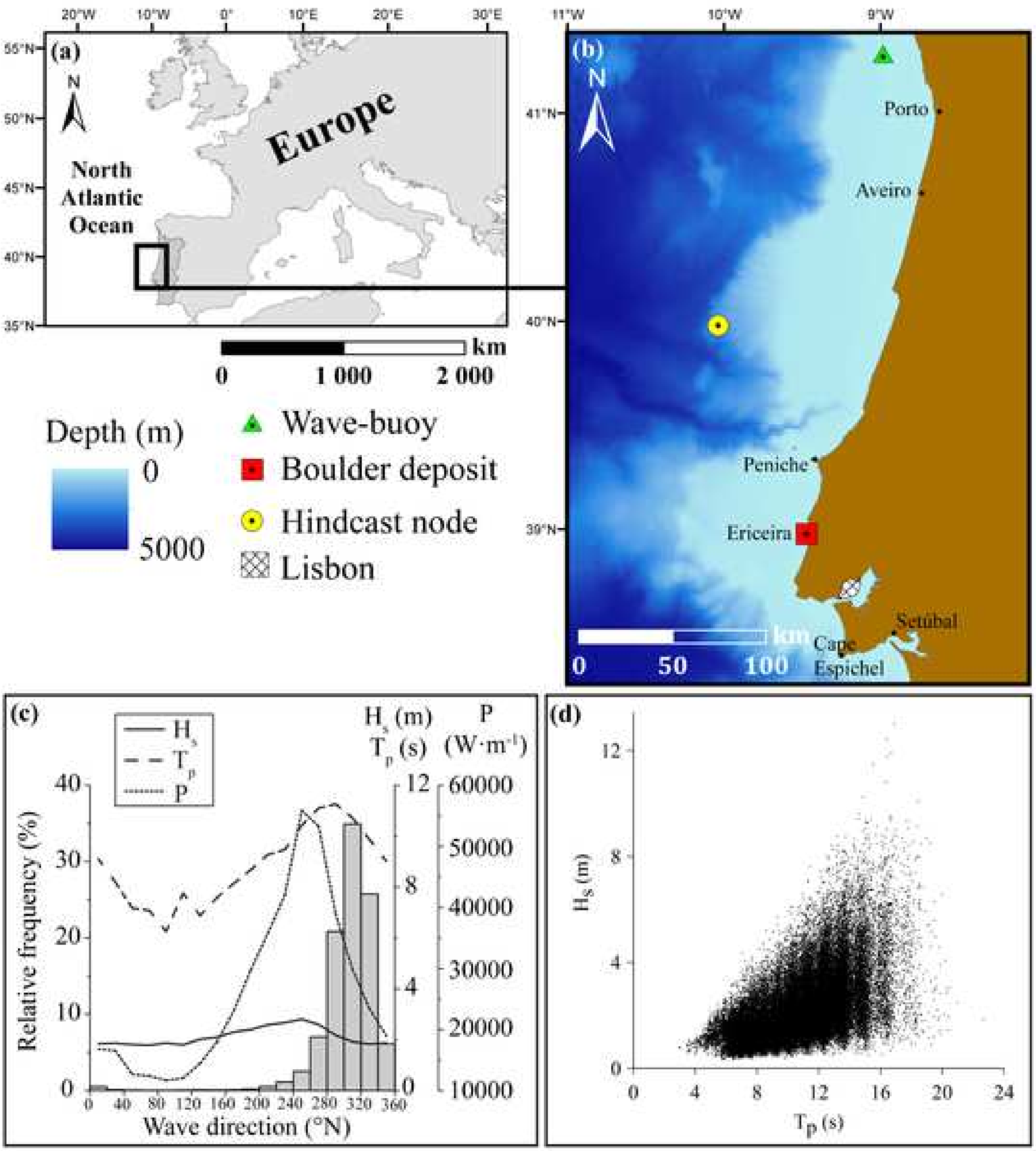
(a)
N
North Atlantic Ocean
Europe
20°W
10°W
0°
10°E
20°E
30°E
55°N
50°N
45°N
40°N
35°N
km
0
1 000
2 000
Depth (m)
0
5000
Wave-buoy
Boulder deposit
Hindcast node
Lisbon
(b)
N
11°W
10°W
9°W
41°N
40°N
39°N
Porto
Aveiro
Peniche
Ericeira
Setubal
Cape Espichel
km
0
50
100
(c)
H_s
T_p
P
H_s (m)
T_p (s)
P
(W·m^{-1})
Relative frequency (%)
Wave direction (°N)
(d)
H_s (m)
T_p (s)

Fig2

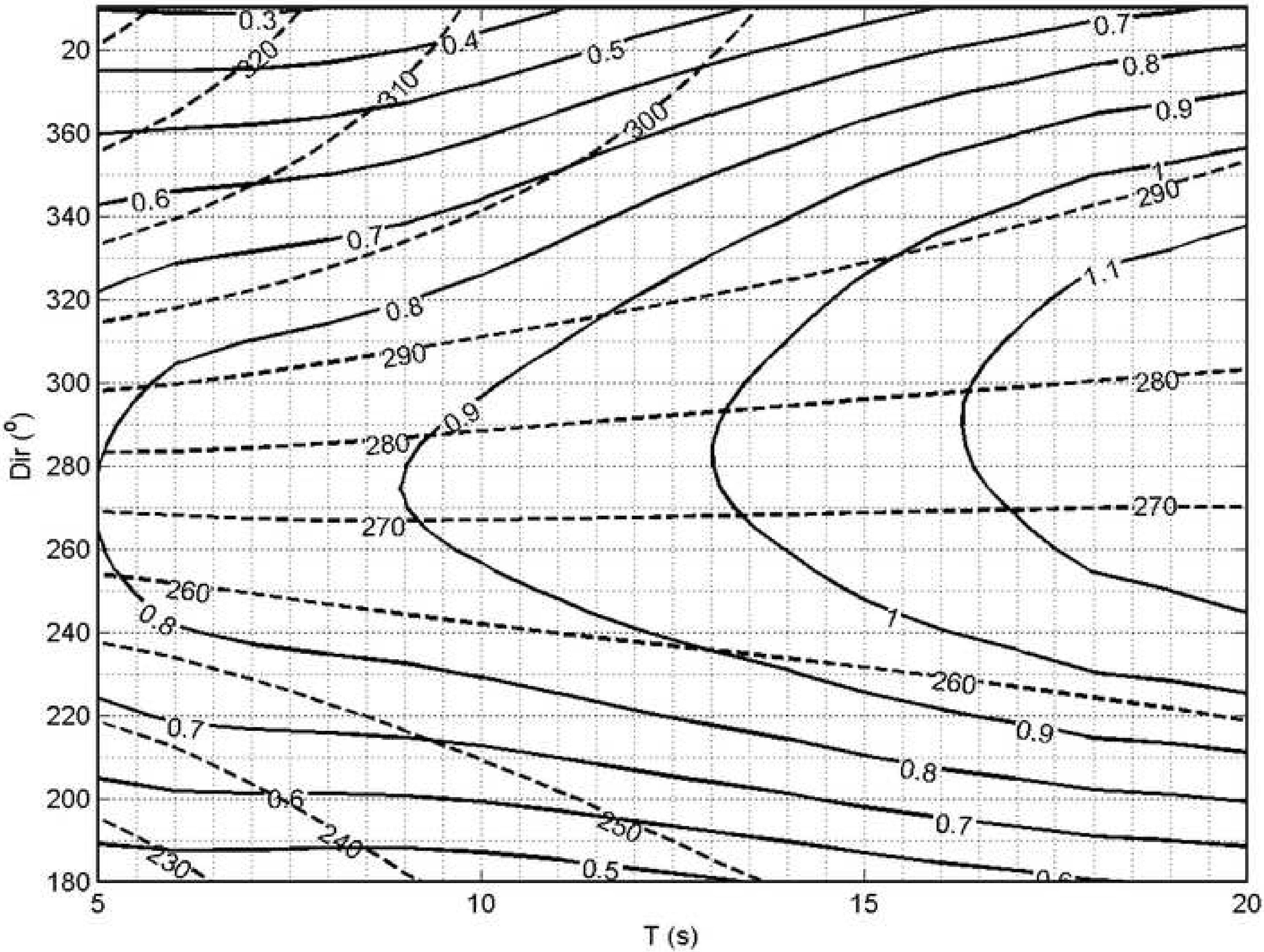
Dir (°)
T (s)
20
360
340
320
300
280
260
240
220
200
180
5
10
15
20
0.3
0.4
0.5
0.6
0.7
0.8
0.9
1
1.1
320
310
300
290
280
270
260
250
240
230

Fig3

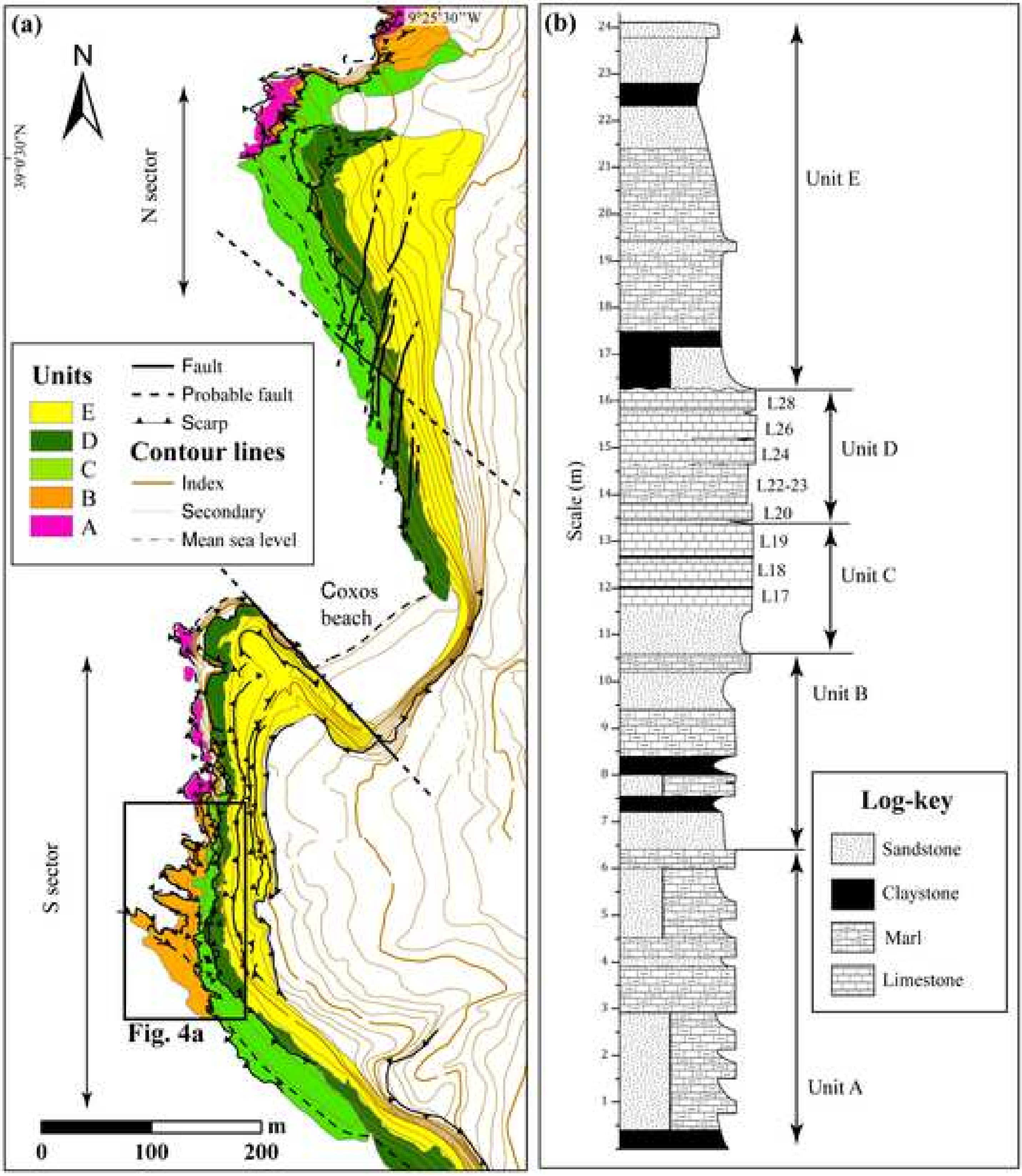
(a)
N
9°25'30''W
39°0'30''N
N sector
S sector
Units
E
D
C
B
A
Fault
Probable fault
Scarp
Contour lines
Index
Secondary
Mean sea level
Coxos
beach
Fig. 4a
0
100
200
m
(b)
Scale (m)
1
2
3
4
5
6
7
8
9
10
11
12
13
14
15
16
17
18
19
20
21
22
23
24
Unit E
L28
L26
L24
L22-23
L20
Unit D
L19
L18
L17
Unit C
Unit B
Unit A
Log-key
Sandstone
Claystone
Marl
Limestone

Fig4

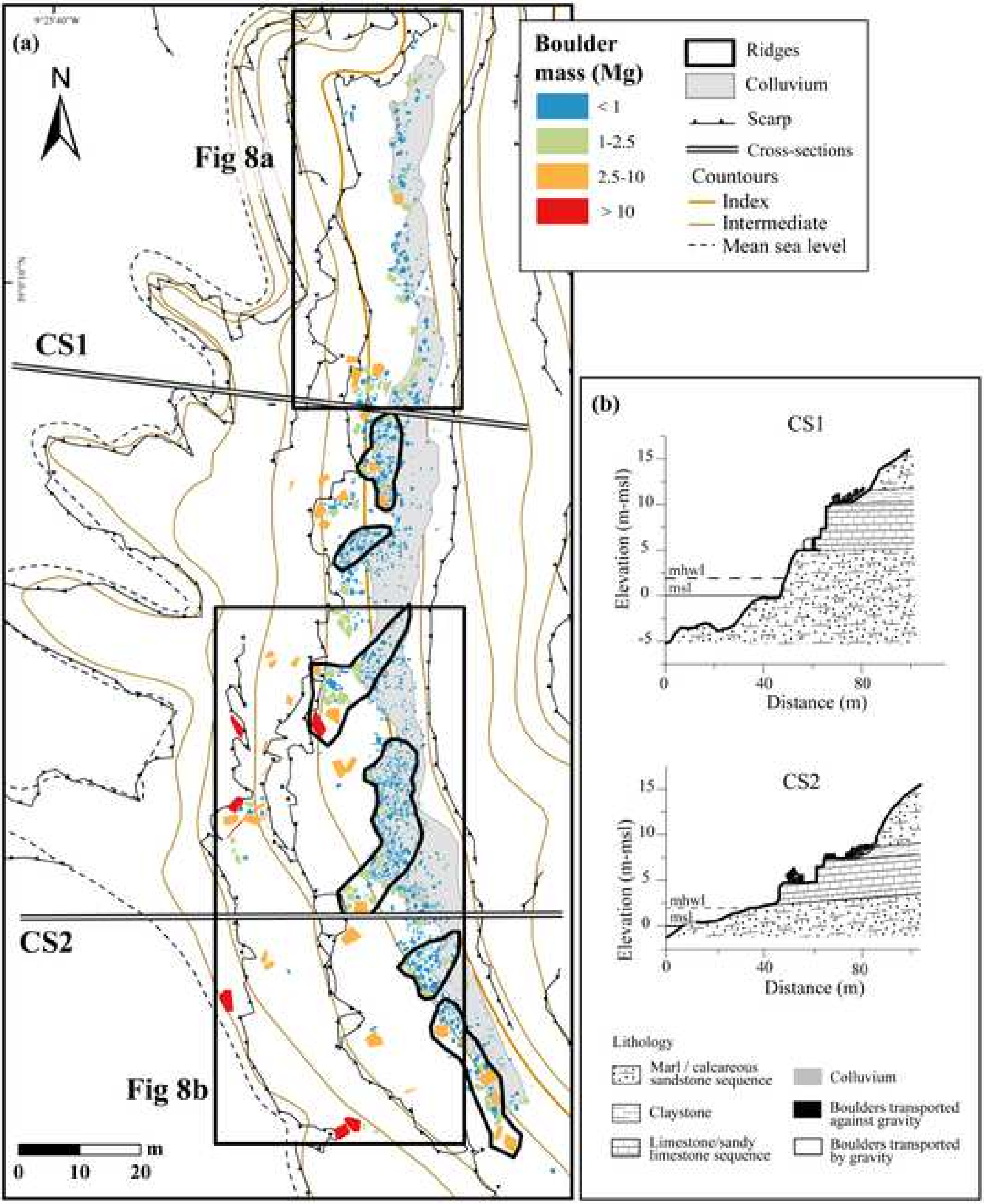

(a)
N
Fig 8a
CS1
CS2
Fig 8b
m
0 10 20
Boulder mass (Mg)
< 1
1-2.5
2.5-10
> 10
Ridges
Colluvium
Scarp
Cross-sections
Countours
Index
Intermediate
Mean sea level
(b)
CS1
Elevation (m-msl)
mhwl
msl
Distance (m)
CS2
Elevation (m-msl)
mhwl
msl
Distance (m)
Lithology
Marl / calcareous sandstone sequence
Claystone
Limestone/sandy limestone sequence
Colluvium
Boulders transported against gravity
Boulders transported by gravity

Fig5

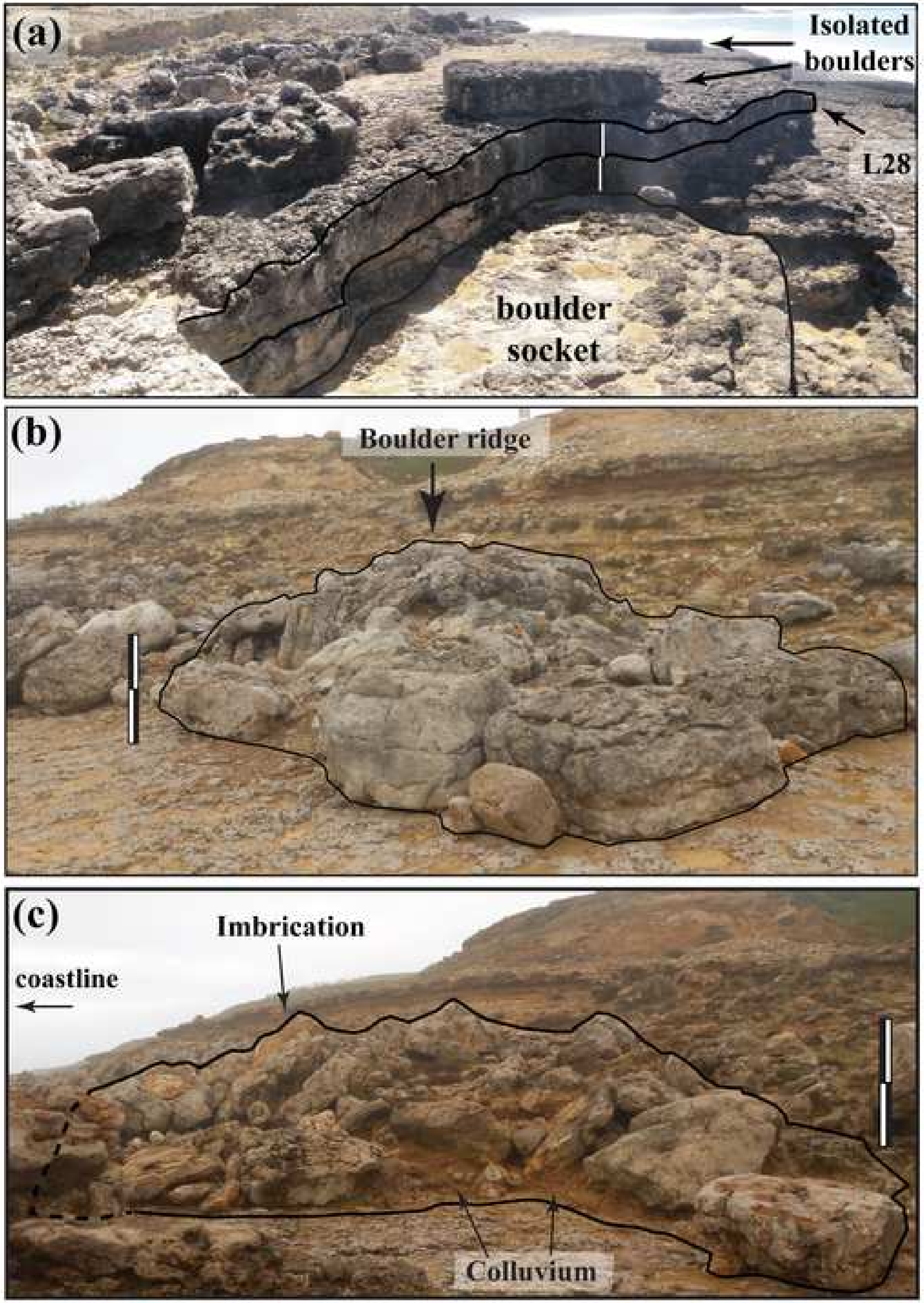

(a)
Isolated
boulders
L28
boulder
socket
(b)
Boulder ridge
(c)
Imbrication
coastline
Colluvium

Fig6

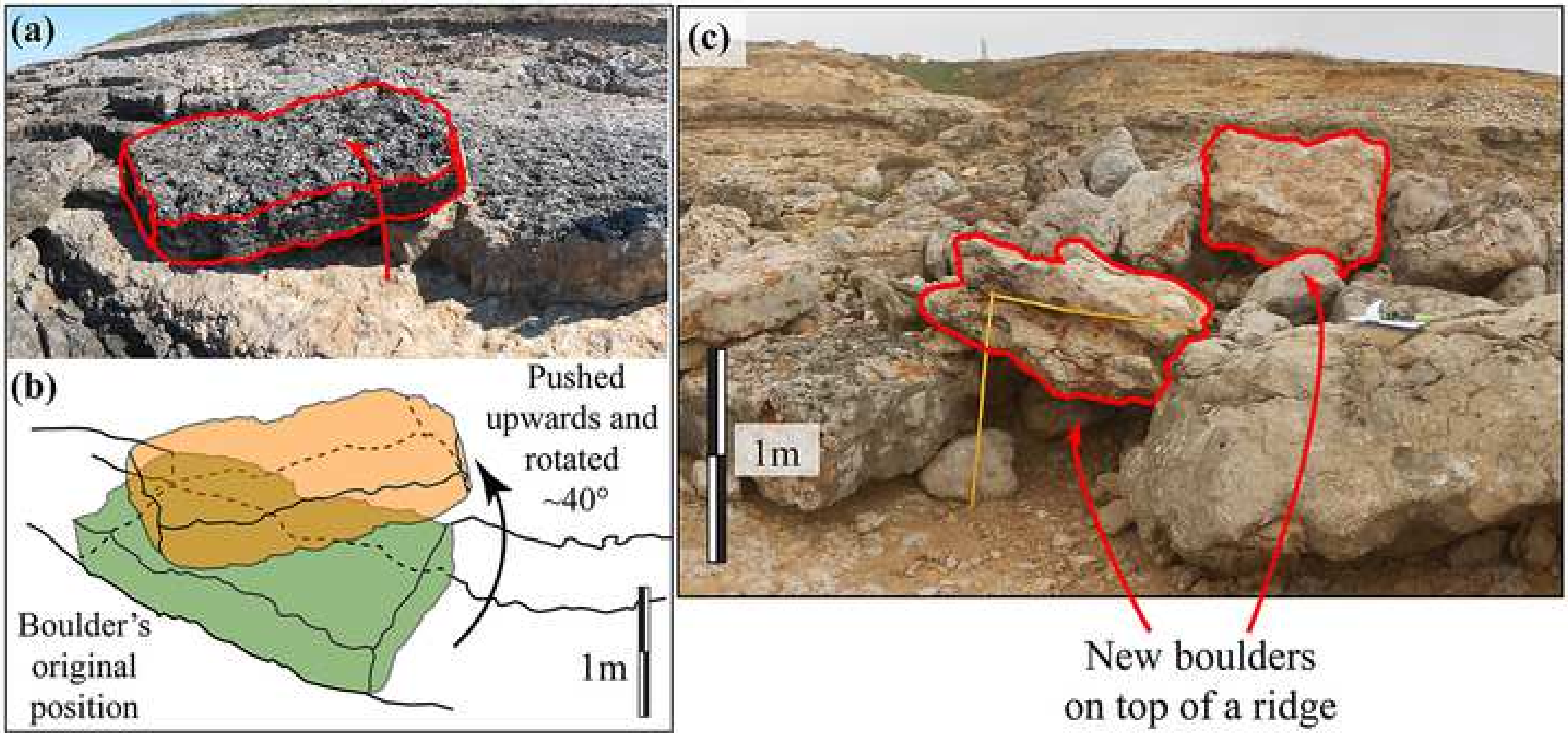
(a)
(b)
Pushed upwards and rotated ~40°
Boulder's original position
1m
(c)
1m
New boulders on top of a ridge

Fig7

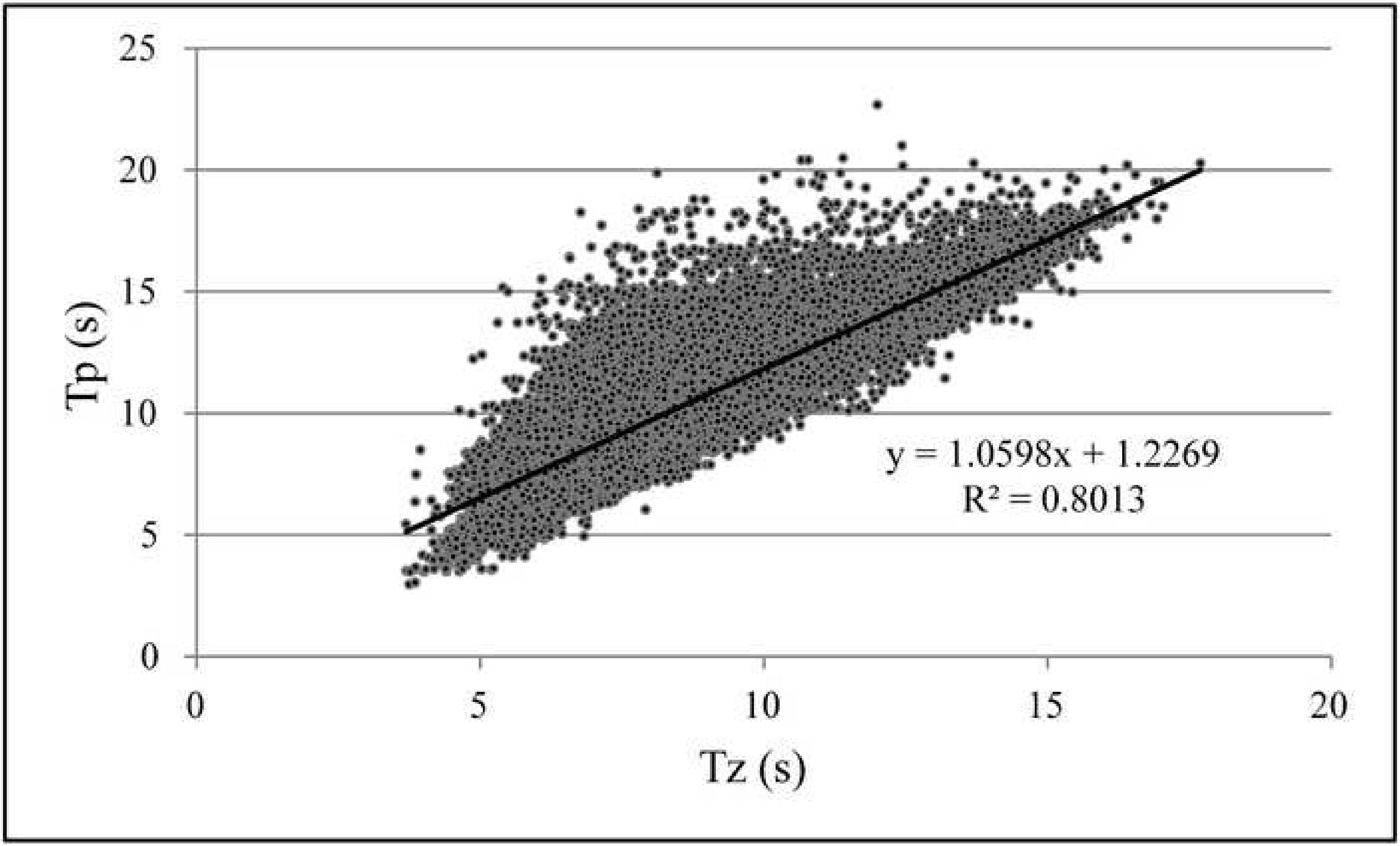

Fig8

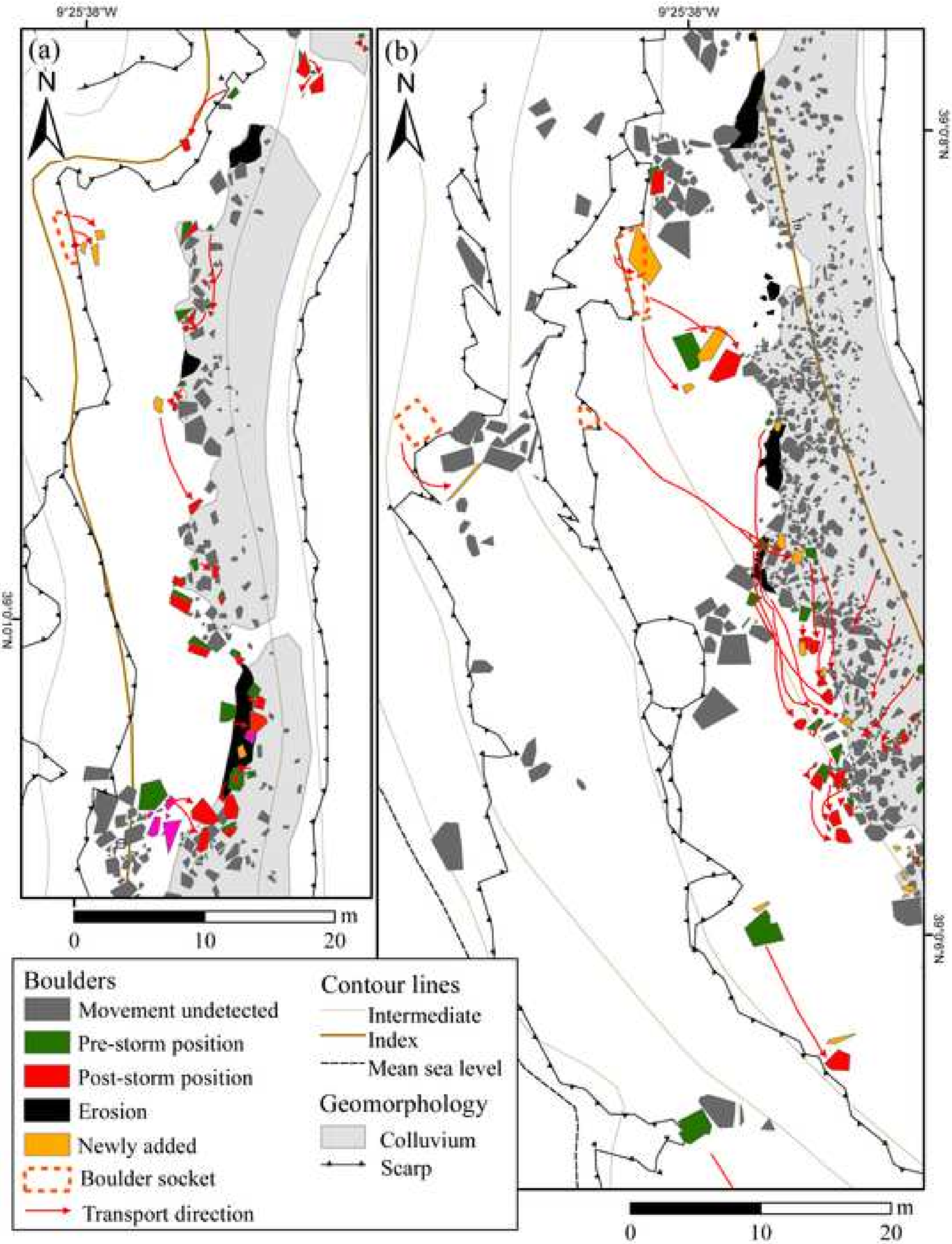
9°25'38"W
(a)
N
39°1'0"N
0
10
20
m
9°25'38"W
(b)
N
39°0'0"N
39°0'6"N
0
10
20
m
Boulders
Movement undetected
Pre-storm position
Post-storm position
Erosion
Newly added
Boulder socket
Transport direction
Contour lines
Intermediate
Index
Mean sea level
Geomorphology
Colluvium
Scarp

Fig9

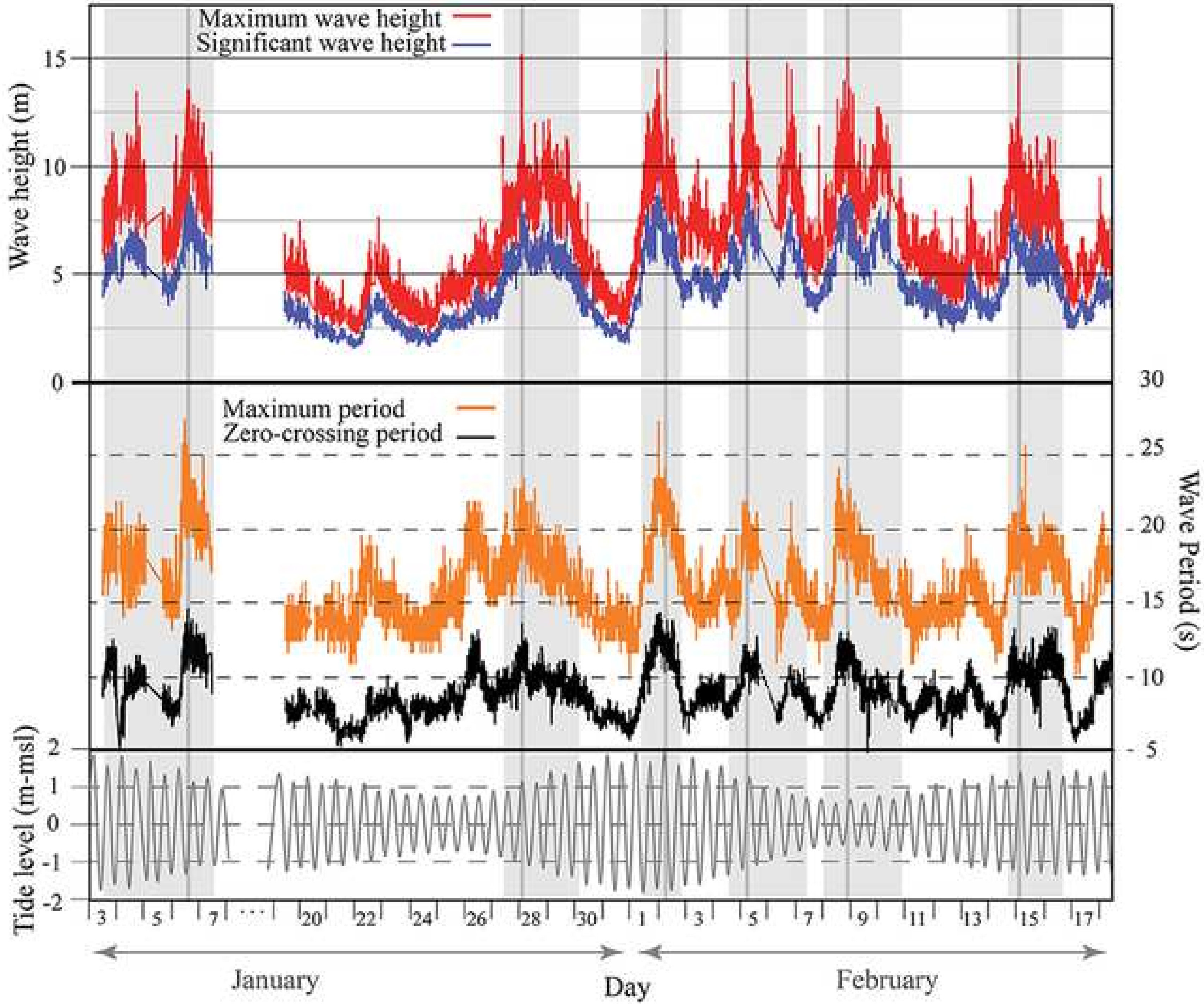
Maximum wave height
Significant wave height
Wave height (m)
15
10
5
0
Maximum period
Zero-crossing period
30
25
20
15
10
5
Wave Period (s)
Tide level (m-msl)
2
1
0
-1
-2
3
5
7
...
20
22
24
26
28
30
1
3
5
7
9
11
13
15
17
January
Day
February

Fig10

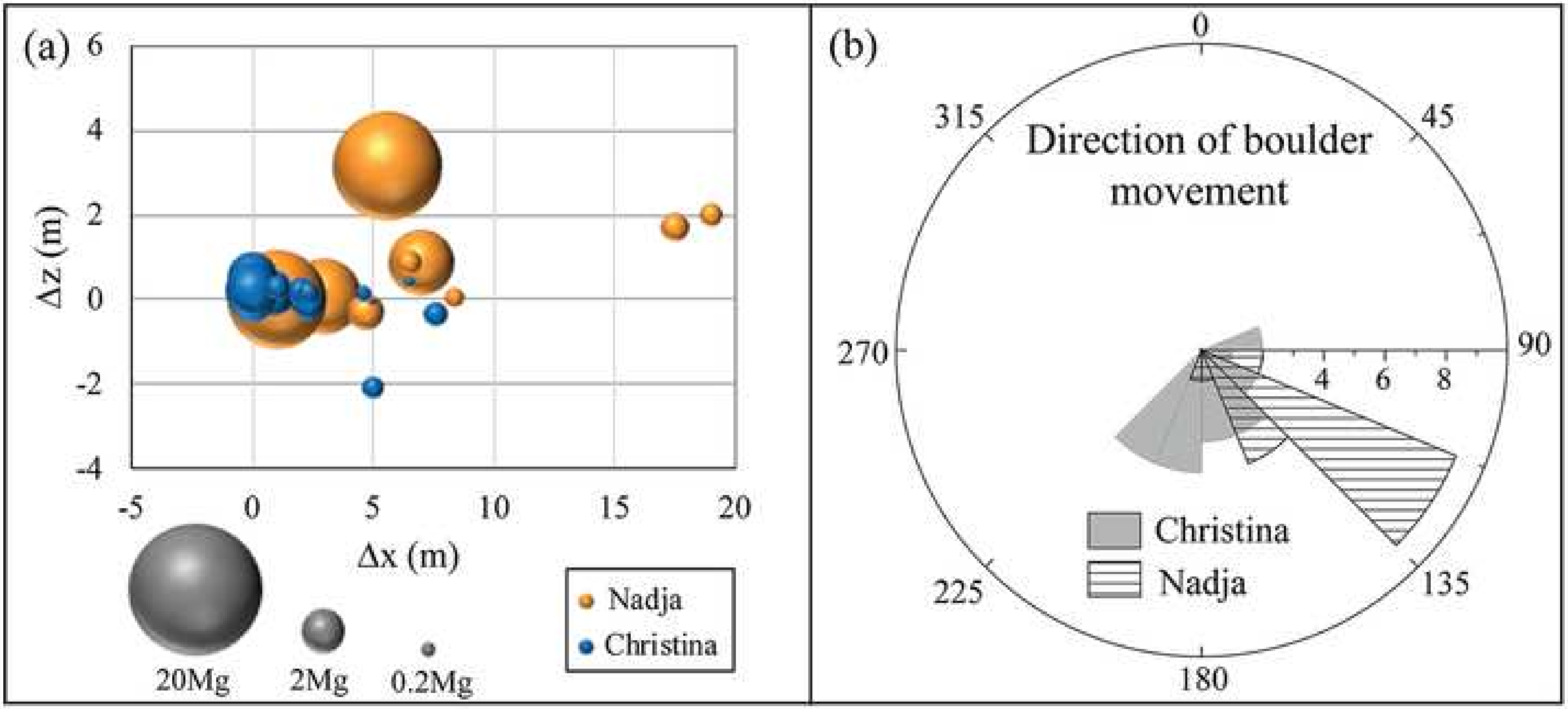

(a)
Δz (m)
6
4
2
0
-2
-4
-5
0
5
10
15
20
Δx (m)
20Mg
2Mg
0.2Mg
Nadja
Christina
(b)
0
45
90
135
180
225
270
315
Direction of boulder movement
4
6
8
Christina
Nadja

Fig11

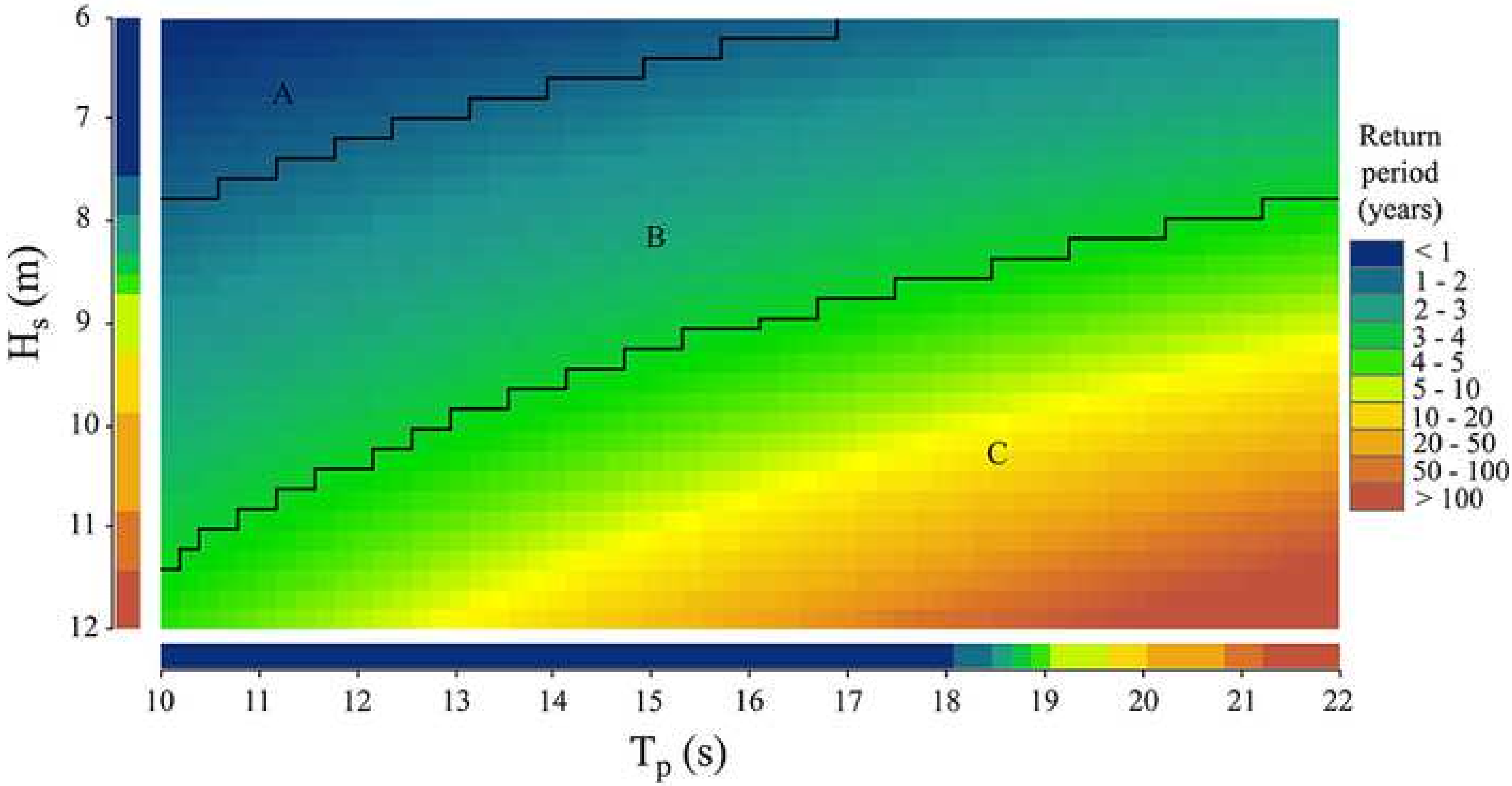

A
B
C
6
7
8
9
10
11
12
Hs (m)
10
11
12
13
14
15
16
17
18
19
20
21
22
Tp (s)
Return period (years)
< 1
1 - 2
2 - 3
3 - 4
4 - 5
5 - 10
10 - 20
20 - 50
50 - 100
> 100

FigS1 Supporting information

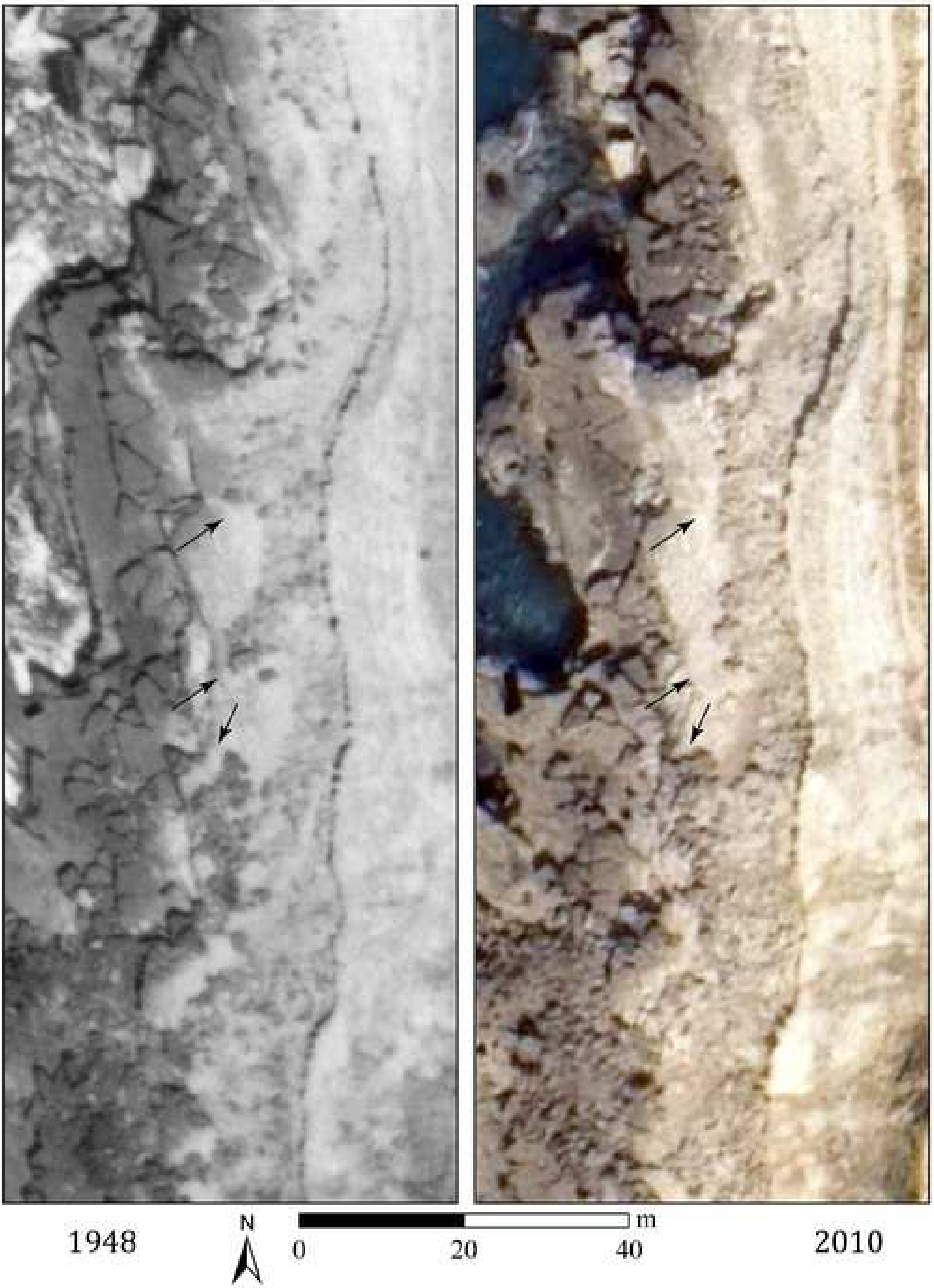

FigS2 Supporting information

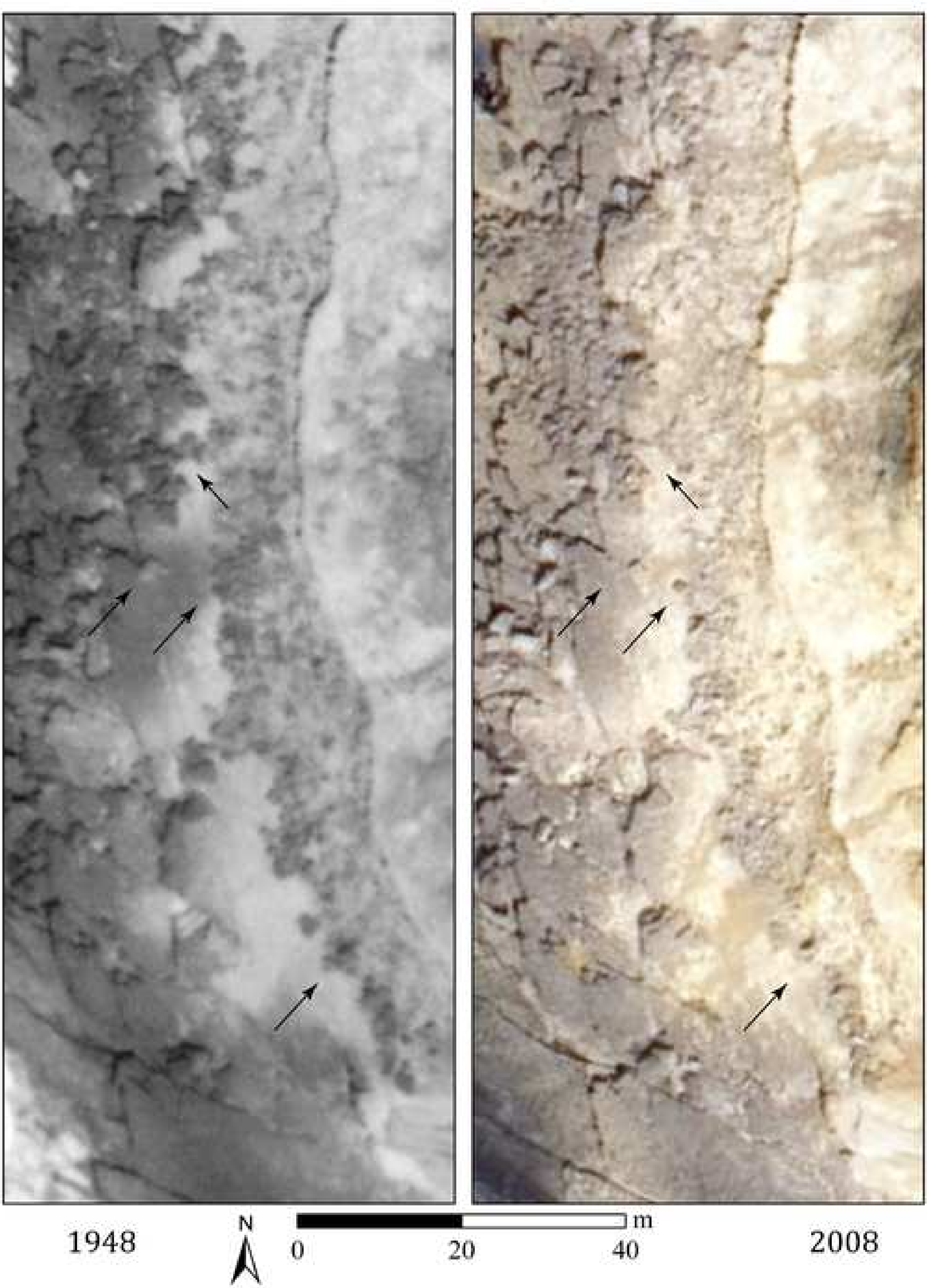

FigS3 Supporting information